PHYSICAL REVIEW D VOLUME 22, NUMBER 1 1 JULY 1980

Forward hard scattering in hadron-hadron collisions in the energy region $\sim 10^{14}$ eV

Toru Shibata
Department of Physics, Aoyama Gakuin University, 6-16-1, Chitosedai, Setagaya-ku, Tokyo 157, Japan
(Received 13 December 1979)

On the basis of the quark-parton picture, we derive analytically the cross sections for production of hadrons and γ rays through forward hard scattering in hadron-hadron collisions in the energy region $\sim 10^{14}$ eV. We take account of transverse motions both of partons inside proton $(\vec{p}_T)_{p\to q}$, and of hadrons fragmented from quark (gluon) $(\vec{k}_T)_{q\to h}$. In addition, we take the effects of scale violation into account. We compared the numerical results thus obtained with cosmic-ray data in the energy region $\sim 10^{14}$ eV, observed at Mt. Chacaltaya by Japan-Brazil emulsion-chamber collaboration. After eliminating carefully the bias effect inherent there, we found the theoretical calculations reproduced surprisingly well the cosmic-ray data on large $p_{T\gamma}$ not only in the shape, but also in the absolute value. We obtain also the production cross sections of π^+ and K^+ expected from the forthcoming $\bar{p}$-p colliding beams with $\sqrt{s} = 540$ GeV at Fermilab and CERN in the early 1980's, with use of the formula derived in the present paper.

I. INTRODUCTION

Phenomena of large transverse momentum were discovered more than fifteen years ago from cosmic-ray-beam interactions in the atmosphere, particularly from emulsion-chamber (hereafter called EC) and air-shower array experiments,[1] and soon more direct evidences of those were subsequently found in EC data with use of the local target layer.[2] Since then, many cosmic-ray physicists have recognized that the large-p_T phenomena play a dominant role in ultra-high-energy physics, and may bring us critical information on the deep structure of elementary particles.

In 1973, a large-p_T phenomena were definitely confirmed by CERN ISR experiment.[3] As soon as the extraordinary tail of large p_T was reported, most people considered that it had arisen from the point-point interaction between fundamental constituents (partons[4]), one from the projectile and the other from the target, just in the same way as the historical evidence that the existence of a nucleus inside the atom was dramatically confirmed by Rutherford large-angle scattering. As is well known, if so, the cross section of the large p_T should fall like p_T^{-4}. Nevertheless, subsequent accelerator experiments on large p_T have never exhibited p_T^{-4} law, but gave p_T^{-8} law a result which made many physicists discouraged about the point-point interaction approach to hadronic large-p_T phenomena.

In order to explain p_T^{-8} behavior, many theoretical physicists have proposed various models until now, making the original point-point interaction approach somewhat modified, such as the quark-quark hard-scattering "black-box" model,[5] constituent-interchange model,[6] and so on. They succeeded in getting reasonable agreement with experimental data, though they were not successful for correlation data, particularly on jet structure in away side triggered by large-p_T particle in toward side.

Recently, Feynman, Field, and Fox[7] applied quantum chromodynamics (QCD) for large-p_T phenomena in hadron-hadron collisions and reproduced experimental data well, not only on the single-particle cross section, but also on the various correlation data. According to them, the p_T^{-8} behavior of experiment would be "accidental" and not fundamental. The reason why the p_T^{-8} "law" is observed experimentally instead of the p_T^{-4} law may be summarized as follows:

(i) Transverse motion of quarks (gluons) within colliding hadrons $(\vec{p}_T)_{p\to q}$, and that of hadrons produced by quark (gluon) successive decay $(\vec{k}_T)_{q\to h}$.

(ii) Scale violation on the structure function $G(x, Q^2)$ and on the decay function $D(z_c, Q^2)$, generated by gluon corrections typified by bremsstrahlung and quark-antiquark pair production processes, where Q^2 is some characteristic momentum in collision.

(iii) Q^2 dependence of the effective coupling constant $\alpha_s(Q^2)$, which decreases logarithmically with increasing Q^2.

The experimental evidences of the former two, (i) and (ii), are now indisputable, for instance, high ratio of σ_L/σ_T (Ref. 8) $(\simeq 4\langle p_T^2\rangle_{p\to q}/Q^2)$ and x distribution with Q^2 dependence[9] observed by lepton-hadron collision, though not enough on z_c distribution with Q^2 dependence, in particular at large Q^2.

From the theoretical point of view, the above three, (i), (ii), and (iii), are naturally expected from QCD. The violation of Bjorken scaling is explained by higher-order corrections for point-point interaction, for instance, those due to the bremsstrahlung emission of gluon from quark, and the pair production of quark-antiquark from gluon. Recent discovery[10] of three-jet emissions in e^+-e^- collision also gives strong support for the QCD prediction.

Nowadays, many people expect that QCD might be the leading candidate for the underlying theory behind all kinds of interactions, lepton-initiated ones as well as hadron-hadron ones. From the experimental point of view, however, there still remain many problems to be checked further. Above all, tests of QCD at $s \to \infty$ with $Q^2 \gg$ (nucleon mass)^2 bring us invaluable information on the validity of asymptotic free picture, where nonasymptotic effects disappear and p_T^{-4} law may really be observed in the extremely-large-p_T region.

In the present paper, we study large-p_T phenomena in the energy region of $\sqrt{s} \sim 500$ GeV, using cosmic-ray-beam interactions obtained by Japan-Brazil emulsion-chamber collaboration (JBC),[11] high enough beyond the energy range nowadays available at ISR.

In Sec. II, we briefly mention the structure of EC with the local target layer, and in detail the features of EC data, particularly bias effects inherent there, which must be eliminated in order to compare them with theoretical calculations presented in Sec. III.

The large p_T of γ rays concerned here being at most of the magnitude ~2.5 GeV/c, the contribution of the soft γ rays with small $p_{T\gamma}$ must be carefully taken into account. So in Sec. II E, we discuss the background of those in EC data as well as those at ISR.

In Sec. III, we derive analytically the production cross sections of hadron and γ ray in the region $\hat{s} \gg -\hat{t} \gtrsim M_N{}^2$, where $\hat{s}$ and $\hat{t}$ are usual invariants in the quark (gluon)–quark (gluon) hard-scattering system, and M_N is the nucleon mass. We take both effects of the transverse motion of constituents inside proton and scale violation into account. The condition of $\hat{s} \gg -\hat{t}$ makes the analytical calculations quite easy.

In Sec. IV A, we present explicit parametrizations for $G(x, Q^2)$ and $D(z_c, Q^2)$, determined empirically so as to be consistent with experimental data on scale violation found in deep-inelastic collisions. In Sec. IV B, we demonstrate numerical results in the production cross sections of π^+ and K^+ in the range of $p_T = 1-10$ GeV/c at $\sqrt{s} = 540$ GeV. In Sec. IV C, we show results of the numerical calculations on the production cross section of γ ray in the EC energy region, and compare them with the experimental data obtained by JBC on transverse momentum and fractional energy distributions of γ rays.

Section V is reserved for concluding remarks.

II. EMULSION CHAMBER AND PRODUCTION CROSS SECTION OF γ RAY

A. Two-story emulsion chamber

Details of EC, in particular on structure, sensitivities of x-ray film and nuclear emulsion, and energy determination, have been already explained enough in numerous past papers.[12] So we mention here briefly the outline of two-story EC relevant in the present paper.

The two-story EC was designed so as to eliminate uncertainties of interaction point, smearing due to successive nuclear interactions and electromagnetic cascade processes. As demonstrated in Fig. 1, the chamber is composed of four basic parts: upper EC, producer-target (petroleum pitch $C_{26}H_{52}$), air-gap spacer, and lower EC.

The upper chamber consists of an alternate sandwich of a 1.3-cm lead plate (≃2.8 radiation length) and two sheets of Sakura N-type film (high sensitivity), sometimes together with one sheet of Sakura RR-type film (low sensitivity), and with a plate of nuclear emulsion (very low sensitivity). Usually the thickness of the total lead plates is 6–8 cm, thick enough to absorb atmospheric electromagnetic components ($e^\pm$ and γ), which may bring us otherwise a noise in the lower chamber to detect a jet occurring within the producer-target [so-called carbon jet (C jet)].

In the lower chamber, plates of nuclear emulsion are always inserted in every layer to investi-

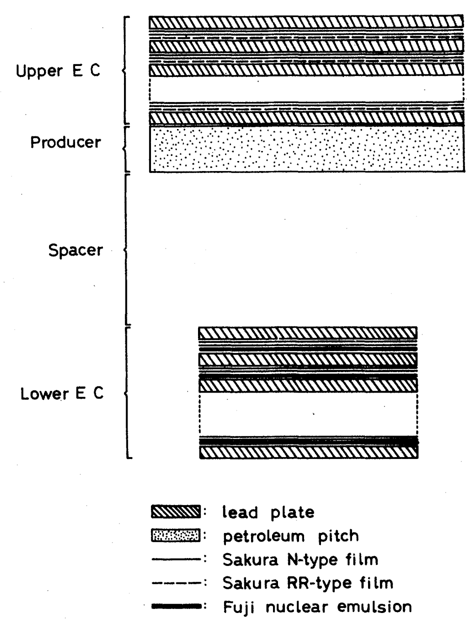

FIG. 1. Schematic view of two-story emulsion chamber.

gate the fine structure of γ rays emitted within the target.

Experiments with this type of EC were started at Mt. Chacaltaya in 1965 by JBC,[13] and were extended in 1970 to their full scale [called chamber (CH) 15].[14] Since the thickness of the producer-target (23 cm) of CH 15 was thin enough in comparison with that of the air-gap spacer (158 cm), it was possible to check the energy calibration with use of $\pi^0 \to 2\gamma$ kinematics. This confirmed[14] that the accuracy of the energy determination of each γ ray with use of the track-counting method is 10~20%, and besides showed a clear peak of π^0 mesons in the invariant mass distribution of a pair of γ rays.

Until now, this type of chamber has been exposed five times at Mt. Chacaltaya. Data used in the present paper are a part of those obtained by four chambers, CH's 15, 16, 17, and 18.

B. Range of interaction energy

Unfortunately, we cannot get directly the energy E_0 of incident beam, but instead observe the energy flow $\sum E_\gamma$ radiated into γ rays, which originate mostly from $\pi^0 \to 2\gamma$ decay. The relation between E_0 and $\sum E_\gamma$ is given by

$$\sum E_\gamma = k_\gamma E_0 , \tag{2.1}$$

here k_γ is inelasticity transferred into γ rays. k_γ is related to the total inelasticity K_{tot} and charge fluctuation ζ_{π^0} in the form of $k_\gamma = \zeta_{\pi^0} K_{\text{tot}}$. If the energy E_0 of the incident nucleon beam is monoenergetic, and if events of C jet are selected without bias, the mean value of k_γ is expected to be $\sim\frac{1}{6}$, assuming $\langle K_{\text{tot}}\rangle = 0.5$ and $\langle \zeta_{\pi^0}\rangle = \frac{1}{3}$, reasonable values confirmed from both experiments of accelerator[15] and cosmic ray.[16]

Now the trigger condition of secondary γ rays in the case of EC experiments is quite different from that in the case of accelerator inclusive-experiments in two senses. The first one is that the energy of incident beam in the former has powerlike spectrum, expressed by $E_0^{-\gamma}$ with $\gamma \simeq 1.8$[17] in the integral form. The second one is that the events are selected by the magnitude of interaction energy $\sum E_\gamma$ released into γ rays.

These trigger conditions lead inevitably to selection of events with larger energy flow $\sum E_\gamma$, so that the inelasticity k defined by Eq. (2.1) is biased larger. Let us write such biased k_γ as $k_{\gamma\,\text{bias}}$.

Now, what we would like to know is the average energy of the incident beam when observing some energy flow $\sum E_\gamma$. Putting the inelasticity distribution of k_γ as $\eta(k_\gamma)dk_\gamma$, we find

$$\langle E_0\rangle = \int_{\Sigma E_\gamma}^{\infty} dE_0 E_0 E_0^{-\gamma-1} \int_{\Sigma E_\gamma/E_0}^{1} dk_\gamma \eta(k_\gamma) \Big/ \int_{\Sigma E_\gamma}^{\infty} dE_0 E_0^{-\gamma-1} \int_{\Sigma E_\gamma/E_0}^{1} dk_\gamma \eta(k_\gamma)$$
$$= [\langle k_\gamma^{\gamma-1}\rangle / \langle k_\gamma^{\gamma}\rangle] \sum E_\gamma , \tag{2.2a}$$

with

$$\langle k_\gamma^{\gamma}\rangle = \int_0^1 dk_\gamma k_\gamma^{\gamma} \eta(k_\gamma) , \tag{2.2b}$$

that is,

$$\langle k_\gamma\rangle_{\text{bias}} = \langle k_\gamma^{\gamma}\rangle / \langle k_\gamma^{\gamma-1}\rangle , \tag{2.3}$$

showing higher bias as the exponent γ of incident nucleon spectrum increases. For instance, assuming

$$\eta(k_\gamma) = 5(1-k_\gamma)^4 \quad \text{with } \langle k_\gamma\rangle = \tfrac{1}{6} , \tag{2.4}$$

we get

$$\langle k_\gamma\rangle_{\text{bias}} = 0.27\text{–}0.29 \quad \text{for } \gamma = 1.8\text{–}2.0 , \tag{2.5}$$

much bigger than the nonbiased case $\langle k_\gamma\rangle = \frac{1}{6}$. Hereafter we call $B = \langle k_\gamma\rangle_{\text{bias}}/\langle k_\gamma\rangle$ the bias factor. Though the value given by Eq. (2.5) may be slightly affected by the choice of the distribution form for $\eta(k_\gamma)$, as well as that of the exponent γ, it seems quite certain that $\langle k_\gamma\rangle_{\text{bias}}$ lies around $\frac{1}{4} \sim \frac{1}{3}$, in agreement with the results of Monte Carlo calculations performed by several authors.[18]

Now, as the energy flow $\sum E_\gamma$ studied in the present paper ranges from 20 to 120 TeV with the average value $\langle \sum E_\gamma\rangle = 40.0$ TeV, the energy of incident beam in the laboratory system (LS) becomes

$$E_0 = 72.5\text{–}435 \text{ TeV} \quad \text{with } \langle E_0\rangle = 145 \text{ TeV} , \tag{2.6}$$

choosing $\langle k_\gamma\rangle_{\text{bias}} = 0.28$.

The energy in the center-of-mass system (cms) corresponds to

$$\sqrt{s} = 396\text{–}964 \text{ GeV with } \langle \sqrt{s}\,\rangle = 523 \text{ GeV} , \tag{2.7}$$

high enough beyond the energy range available nowadays at ISR.

C. Range of emission angle and scaling variable

As is well known, the emission angle θ_γ^* in cms is related to the angle θ_γ ($\ll 1$) in LS,

$$\tan\frac{\theta_\gamma^*}{2} \simeq \gamma_c \theta_\gamma \simeq \left(\frac{\sum E_\gamma}{2M_N k_\gamma}\right)^{1/2} \theta_\gamma , \tag{2.8}$$

where γ_c is the Lorentz factor of cms relative to LS, and M_N is the nucleon mass. Let us show the distribution of $\theta_\gamma(\sum E_\gamma)^{1/2}$ for observed γ rays with $E_\gamma \geq 0.0125 \sum E_\gamma$ (discussed later) and with $p_{T\gamma} \geq 500$ MeV/c, obtained by C-jet data, in Fig. 2. One finds there the maximum value of $\theta_\gamma(\sum E_\gamma)^{1/2}$ lies around 0.15–0.20 rad $\sqrt{\text{GeV}}$, so that most of the γ rays are produced within the forward cone ~20° in cms.

We have ~1200 single γ rays with $E_\gamma \gtrsim 0.2$ TeV, which are detected by 71 events of C jet with $\sum E_\gamma \geq 20$ TeV. The maximum transverse momentum of γ ray in those obtained up to date is 2.5 GeV/c[19] corresponding on the average to the range of $p_{T\pi} \lesssim 5$ GeV/c for the transverse momentum of pion.

Cosmic-ray physicists have used a variable $f = E_\gamma / \sum E_\gamma$, fractional energy of γ ray, for a long time, while accelerator physicists have used a scaling variable $z_\gamma = 2p^*_{\gamma L}/\sqrt{s}$ defined in cms. The relation between the above two variables is simply given by

$$z_\gamma \simeq k_\gamma f \tag{2.9}$$

in the region $\theta^*_\gamma \lesssim 20°$.[20]

Naturally, the transverse scaling variable x_T $(=2p_{T\gamma}/\sqrt{s})$ is extremely small, for instance, $x_T \lesssim 10^{-2}$ because of $(p_{T\gamma})_{\max} \sim 2.5$ GeV/c, that is, almost zero.

D. Invariant cross section of γ ray

Let us write down the invariant cross section of γ ray as

$$\phi(E_0, \vec{p}_\gamma) \equiv E_\gamma \frac{d^3\sigma}{d\vec{p}_\gamma{}^3} = \frac{z_\gamma d^2\sigma}{dz_\gamma 2\pi p_{T\gamma} dp_{T\gamma}} . \tag{2.10}$$

We have of course a condition

$$\iint E_\gamma \phi(E_0, \vec{p}_\gamma) \frac{d^3\vec{p}_\gamma}{E_\gamma} = \langle k_\gamma \rangle E_0 \sigma_{\text{inel}} . \tag{2.11}$$

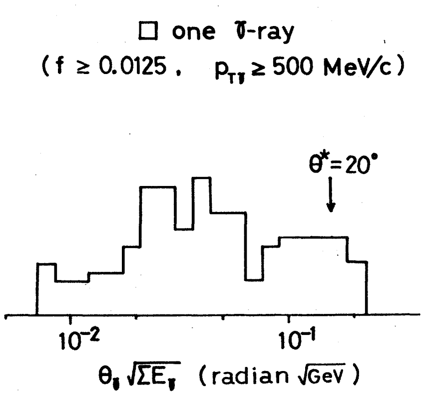

FIG. 2. Histogram of $\theta_\gamma(\Sigma E_\gamma)^{1/2}$ distribution for γ rays with $f \geq 0.0125$ and with $p_{T\gamma} \geq 500$ MeV/c, obtained by two story EC.

Now, the observed cross section $\phi_{\text{obs}}(E_0, \vec{p}_\gamma)$, obtained by C-jet data, is biased as discussed before, that is

$$\iint E_\gamma \phi_{\text{obs}}(E_0, \vec{p}_\gamma) \frac{d^3\vec{p}_\gamma}{E_\gamma} = \langle k_\gamma \rangle_{\text{bias}} E_0 \sigma_{\text{inel}} . \tag{2.12}$$

Since the minimum detection energy of γ ray (~0.2 TeV) is much smaller than the interaction energy (20–120 TeV), we can expect the shape of the distribution function $\phi_{\text{obs}}(E_0, \vec{p}_\gamma)$ is not seriously deformed from the real one $\phi(E_0, \vec{p}_\gamma)$ except in the small region $E_\gamma \lesssim 0.2$ TeV. Then, we get a relation

$$\phi_{\text{obs}}(E_0, \vec{p}_\gamma) \simeq [\langle k_\gamma \rangle_{\text{bias}} / \langle k_\gamma \rangle] \phi(E_0, \vec{p}_\gamma) = B\phi(E_0, \vec{p}_\gamma) . \tag{2.13}$$

That is to say, we must divide the observed cross section $\phi_{\text{obs}}(E_0, \vec{p}_\gamma)$ by the bias factor B in order to get the real cross section. The bias factor B is of the magnitude 1.5–2.0 as expected from the previous discussion.

In Fig. 3 , we present the transverse momentum distribution of γ rays, obtained by the C-jet data in the energy range $\sum E_\gamma = 20 \sim 120$ TeV. The vertical axis represents the production cross section of γ ray *per event* integrated over the fractional energy f,

$$\frac{B}{\sigma_{\text{inel}}} \int_{z_{\gamma\min}}^{1} \frac{z_\gamma d^2\sigma}{dz_\gamma 2\pi p_{T\gamma} dp_{T\gamma}} \frac{dz_\gamma}{z_\gamma}$$

$$= \frac{B}{\sigma_{\text{inel}}} \int_{f_{\min}}^{1} \frac{d^2\sigma}{df\, 2\pi p_{T\gamma} dp_{T\gamma}} df , \tag{2.14}$$

here $z_{\gamma\min} = \langle k_\gamma \rangle_{\text{bias}} f_{\min}$. The experimental points are plotted for three cases, $f_{\min} = \frac{1}{80}$, $\frac{1}{40}$, and $\frac{1}{20}$, which correspond to the sets of minimum detection energies of γ rays, $E_{\gamma\min} = 0.25$, 0.5, and 1.0 TeV, respectively, at $\sum E_\gamma = 20$ TeV, high enough in comparison with the lower limit of detection for individual γ rays 0.1–0.2 TeV. We draw there three curves in small-$p_{T\gamma}$ region together, which are deduced from the well-known $\exp(-6p_T)$ law for the transverse momentum distribution of pion (see next subsection).

It may be interesting to see the exponent n of the above tail found in the region $p_{T\gamma} \gtrsim 500$ MeV/c, in the case of fits to the data of powerlike form $p_{T\gamma}^{-n}$. Figure 4 gives $p_{T\gamma}$ distribution for γ rays with $f \geq \frac{1}{80}$, represented by log-log scale. We find there powerlike behavior with the exponent $n = 4.9$, not $n = 4$, but rather nearer to the value expected from the point-point interaction than the case $n = 8$ found in accelerator energy region.

In Fig. 5, we demonstrate the distribution of fractional energy f $(=z_\gamma/\langle k_\gamma \rangle_{\text{bias}})$ for γ rays with $p_{T\gamma} \geq 750$ and ≥ 850 MeV/c. We draw also back-

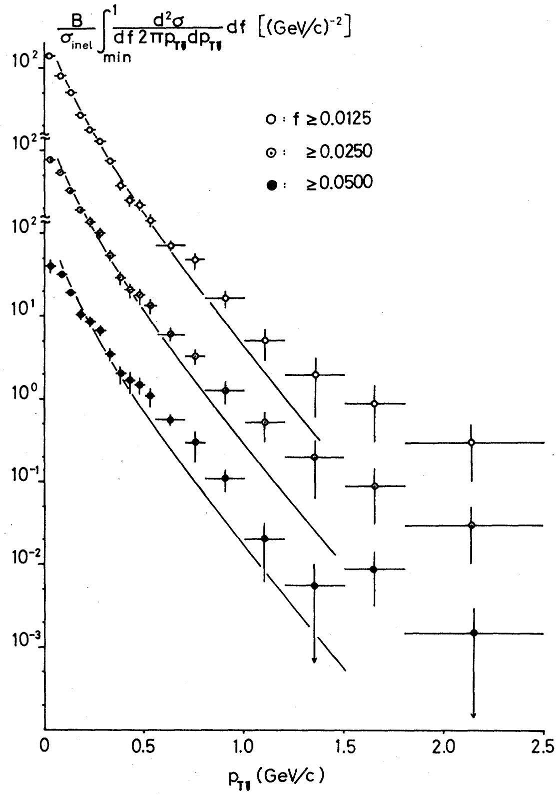

FIG. 3. Transverse-momentum distribution of γ rays per interaction at the energy region $\Sigma E_\gamma = 20$–120 TeV. Vertical axis is integrated over f, where three cases for lower limit of f are presented. Three solid curves are those expected from Eq. (2.16) after integrating over f from 0.0125, 0.025, and 0.05 to 1.

ground curves expected from Eq. (2.16) after integrating with respect to $p_{T\gamma}$ from 750 and 850 MeV/c to infinity. One finds that experimental points lie significantly higher than those expected from the extrapolation of soft γ rays with small $p_{T\gamma}$.

E. Background of soft γ rays with small p_{T_γ}

The biggest transverse momentum of γ ray caught until now by two-story EC with total area ~150 m^2 year at Mt. Chacaltaya is 2.5 GeV/c.[19] So the contribution due to the background soft γ rays with small $p_{T\gamma}$ must be carefully taken into account in the forward region.

Since the distribution functions of pions on p_T and z ($=2p_L^*/\sqrt{s}$) are approximately expressed in the region $p_T \lesssim 1$ GeV/c (Ref. 15) as

$$\frac{d\sigma}{dp_T^2} \propto e^{-6p_T} \text{ and } \frac{d\sigma}{dz} \propto e^{-z/z_{0\pi}}, \qquad (2.15)$$

we assume the following form for the background soft γ rays:

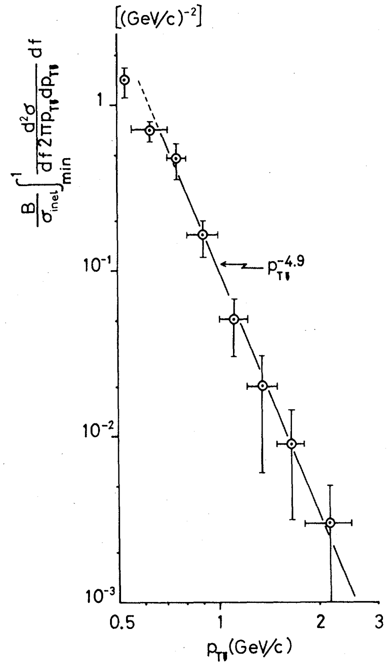

FIG. 4. $p_{T\gamma}$ distribution with $f \geqslant 0.0125$ drawn in the form of log-log scale.

$$\frac{B}{\sigma_{\rm inel}} E_\gamma \frac{d^3\sigma}{d\vec{p}_\gamma^{\,3}} = \frac{A_{\rm bias}}{p_{T\gamma}} e^{-6p_{T\gamma}} e^{-f/f_0} \text{ with } f = E_\gamma / \sum E_\gamma, \qquad (2.16)$$

where B is the bias factor as defined in the last section. The above form was originally suggested by the Bristol-Bombay group[27] through cosmic-ray-beam interactions, and was confirmed also at ISR by Neuhofer *et al.*[22]

Let us show f distributions at $p_{T\gamma} = 0.15$–0.25 GeV/c ($\langle p_{T\gamma}\rangle = 0.19$ GeV/c) in three energy intervals, $\sum E_\gamma = 20$–40, 40–80, and 80–120 TeV, in Fig. 6. One finds that similarity relation holds approximately in these regions, although the statistics in higher-energy intervals $\sum E_\gamma \geqslant 40$ TeV are not enough. The best fit of Eq. (2.16) to the superposed data of the above three intervals yields

$$A_{\rm bias} = 8.02 \text{ GeV}^{-1} \text{ and } f_0 = 0.175. \qquad (2.17)$$

In Fig. 7, we compare z_γ distributions deduced from the above f distributions with those obtained by ISR at $p_{T\gamma} = 0.2$ and 0.4 GeV/c. Here, we assumed $\langle k_\gamma\rangle_{\rm bias} = 0.28$ ($B = 1.68$) in order to convert f into z_γ with use of Eq. (2.9). So, Eq. (2.16) gives the following nonbiased cross-section of γ ray at $\sqrt{s} = 523$ GeV:

$$\frac{1}{\sigma_{\rm inel}} E_\gamma \frac{d^3\sigma}{d\vec{p}_\gamma^{\,3}} = \frac{A}{p_{T\gamma}} e^{-p_{T\gamma}/\langle p_{T\gamma}\rangle} e^{-z_\gamma/z_{0\gamma}}, \qquad (2.18a)$$

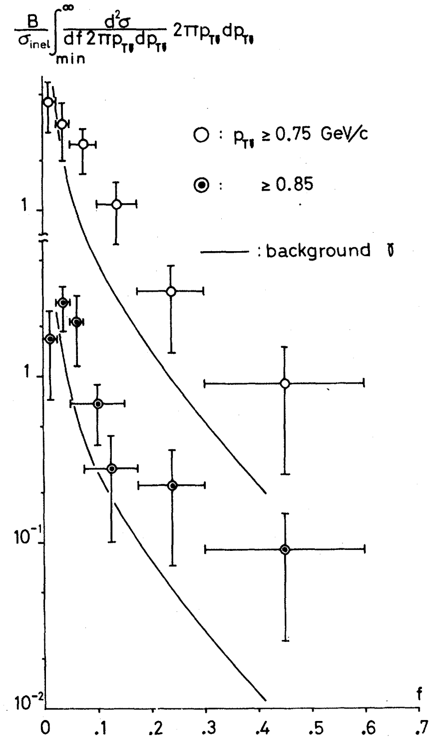

FIG. 5. Distributions of fractional energy $f = z_\gamma/\langle k_\gamma\rangle_{\text{bias}}$ for γ rays with $p_{T\gamma} \geq 750$ MeV/c (open circle) and ≥ 850 MeV/c (open-dotted circle). Two solid curves are those expected from Eq. (2.16) after integrating over $p_{T\gamma}$ from 750 and 850 MeV/c to infinity.

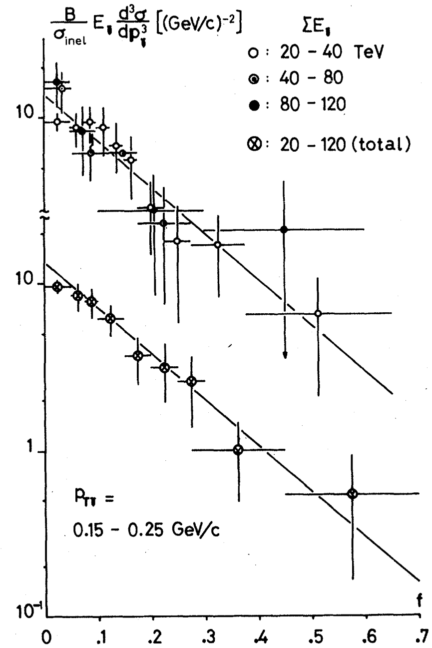

FIG. 6. f distributions at $p_{T\gamma} = 0.15$–0.25 GeV/c with the average value $\langle p_{T\gamma}\rangle = 0.19$ GeV/c, in three energy intervals $\Sigma E_\gamma = 20$–40 TeV (open circle), 40–80 TeV (open-dotted circle), and 80–120 TeV (black circle), together with the superposition of those three (open-crossed circle). Straight lines are those expected from Eq. (2.16) with the numerical constants (2.17).

here,

$$A = A_{\text{bias}}/B = 4.83\ \text{GeV}^{-1}, \quad \langle p_{T\gamma}\rangle = 167\ \text{MeV}/c, \quad z_{0\gamma} = \langle k_\gamma\rangle_{\text{bias}} f_0 = 0.048\,. \tag{2.18b}$$

Figure 7 indicates that the similarity relation does not hold between ISR ($\sqrt{s} \sim 50$ GeV) and C jet ($\sqrt{s} \sim 500$ GeV), even taking the bias effect into account. The parameters A, $\langle p_{T\gamma}\rangle$, and $z_{0\gamma}$ in Eq. (2.18a) at ISR are given as

$$A = 1.48\ \text{GeV}^{-1}, \quad \langle p_{T\gamma}\rangle = 162\ \text{MeV}/c$$

and

$$z_{0\gamma} = 0.083 \quad (\text{Ref. 22})\,. \tag{2.18c}$$

More discussions on the similarity violation will be done in Sec. V.

We present the empirical curves expected from Eq. (2.16) in Fig. 3, after integrating it with respect to f from 0.0125, 0.025, and 0.05 to 1.

F. Composition of incident cosmic-ray beam above chamber

In order to investigate the C-jet data from the viewpoint of the quark-parton picture, we must

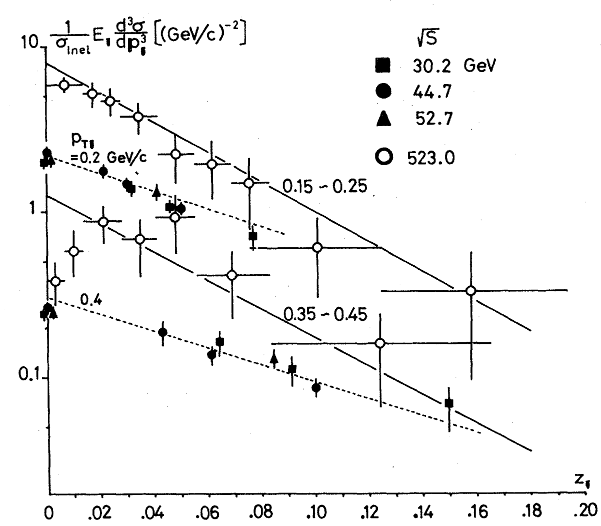

FIG. 7. z_γ distributions of γ rays at $p_{T\gamma} = 0.15$–0.25 GeV/c and 0.35–0.45 GeV/c in C-jet energy region $\langle\sqrt{s}\rangle = 523$ GeV/c, together with those at $p_{T\gamma} = 0.2$ and 0.4 GeV/c in ISR energy region. Solid straight lines are those expected from Eq. (2.18a) with numerical values $A = 4.83$, $\langle p_{T\gamma}\rangle = 167$ MeV/c, and $z_{0\gamma} = 0.048$, while dashed straight lines with $A = 1.48$, $\langle p_{T\gamma}\rangle = 162$ MeV/c, and $z_{0\gamma} = 0.083$.

identify the composition of incident cosmic-ray beam ($p, n, \pi^{\pm}, \ldots$) just falling above the chamber. Unfortunately, experimental data on the particle ratio of cosmic rays in the energy region $\gtrsim 10^{14}$ eV have never been available at mountain level. However, we can estimate analytically various cosmic-ray components, particularly nucleons and charged pions, once setting a model on multiplicity increase of secondary particles produced by nuclear interactions. Now, according to Ref. 20, we show the results of numerical calculations on energy spectrum of nucleon and charged-pion components at Mt. Chacaltaya in Fig. 8. There, we assumed that the multiplicity increases like $\frac{1}{4}$ law, and $\gamma = 1.8$, $\lambda_N = 70$ g/cm^2, and $\lambda_\pi = 100$ g/cm^2,[20] where γ is the exponent of primary cosmic-ray spectrum, and λ_N, λ_π are collision mean free paths of nucleon and charged pion, respectively. The horizontal axis represents the observed energy flow $\sum E_\gamma$ released into γ rays by local nuclear interaction with lead (Pb-jet) and/or pitch (C jet) in chamber. The vertical axis shows flux values of the nucleon and/or the charged pion, which are normalized to one at the nucleon energy $\sum E_\gamma = 1$ TeV.

In Fig. 8, we demonstrate two extreme cases for the charged-pion spectrum. The upper bound corresponds to the case wherein the inelasticity K_π of the nuclear interaction between the charged pion and the air nucleus is catastrophic ($K_\pi = 1$), while the lower one corresponds to the case of uniform distribution from 0 to 1 with $\langle K_\pi \rangle = 0.5$.

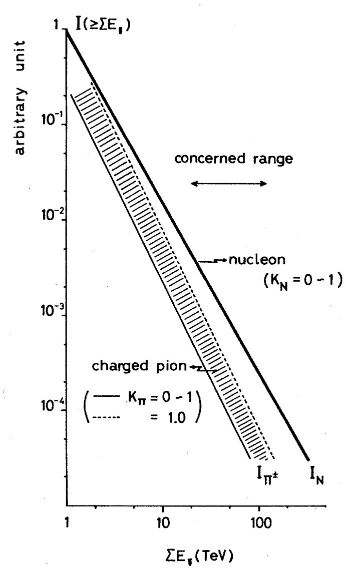

FIG. 8. Integral flux values of nucleon (heavy solid straight line) and charged pions (oblique-lined parts). Horizontal axis denotes the energy released into γ rays by local nuclear interaction within emulsion chamber.

The real situation would be expected to lie between the above two.

One will find in Fig. 8 that the exponent of the charged-pion spectrum is different from that of the nucleon. This is because of the assumption of $\frac{1}{4}$ law on multiplicity increase. Generally, the exponent β of the integral energy spectrum for charged pion and/or γ ray is given by

$$\beta = (\gamma - \alpha)/(1-\alpha) \quad \text{(Ref. 23)}, \tag{2.19}$$

where α is the parameter of multiplicity increase. In fact, the emulsion-chamber experiment indicates[17] that the energy spectrum of γ ray exhibits a slightly steeper exponent than that of the nucleon. So, as the interaction energy of C jet (or Pb jet) gets higher, the contamination of the charged pion becomes smaller. Since the energy range concerned in the present paper is 20–120 TeV, we find from Fig. 8 that the contribution of the charged pion is of the following magnitude:

$$\frac{I_{\pi^\pm}}{I_N + I_{\pi^\pm}} = \begin{cases} 10.9\text{–}29.3\%, & \text{at } \sum E_\gamma = 20 \text{ TeV}, \\ 7.0\text{–}19.6\%, & \text{at } \sum E_\gamma = 120 \text{ TeV}. \end{cases} \tag{2.20}$$

Of course, the above values depend also on the observation levels, that is, they decrease in the upper atmosphere and increase at lower depths. Those are more or less consistent with the results obtained by Sitte *et al.*[35]

Finally, we conclude that the contamination of charged pions is negligibly small (10~20%) in the relevant energy range 20~120 TeV.

One may worry about the beam ratio of protons and neutrons among nucleons falling on the chamber. The present study is, however, aimed at investigating the production cross section of γ rays, mainly from π^0 mesons. Thus, recalling the isospin symmetry for the distribution functions of quarks inside proton and neutron, we do not need to worry about whether the projectile beam is proton or neutron.

III. ANALYTICAL DERIVATION OF PRODUCTION CROSS SECTIONS OF HADRON AND γ RAY ON THE BASIS OF QCD

A. Kinematics

Let us consider a forward hard scattering between constituents a and b of hadrons A (projectile) and B (target), respectively, via the subprocess $a + b \to c + d$. Using the notation in Fig. 9, usual variables x_a, x_b, and x_c are given by

$$p^*_{aL} \simeq x_a P^*, \quad p^*_{bL} \simeq x_b P^*, \text{ and } p^*_{cL} \simeq x_c P^*, \text{ with } 2P^* \simeq \sqrt{s}. \tag{3.1}$$

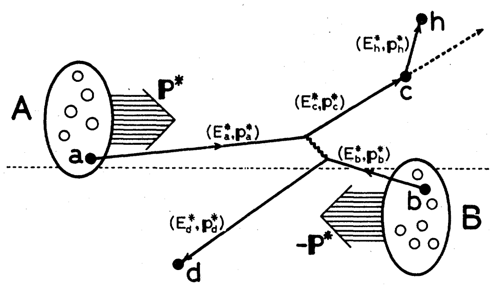

FIG. 9. Hard-scattering mechanism which produces hadron h with large p_T in hadron-hadron collision.

In the forward region, where $p_{aL}^* \gg p_{aT}^*$, $p_{bL}^* \gg p_{bT}^*$, and $p_{cL}^* \gg p_{cT}^*$, the variables $\hat{s}$, $\hat{t}$, and $\hat{u}$ in the two-to-two scattering system are given by

$$\hat{s} = (p_a^* + p_b^*)^2 \simeq x_a x_b s\,, \tag{3.2a}$$

$$\hat{t} = (p_c^* - p_a^*)^2 \simeq -x_a x_c (\vec{p}_{aT}^*/x_a - \vec{p}_{cT}^*/x_c)^2\,, \tag{3.2b}$$

$$\hat{u} = (p_b^* - p_c^*)^2 \simeq -x_b x_c s\,, \tag{3.2c}$$

where mass terms are neglected. Remembering the two-to-two scattering constraints $\hat{s} + \hat{t} + \hat{u} \simeq 0$, we have a condition

$$x_b(x_a - x_c) - x_a x_c (\vec{p}_{aT}^*/x_a - \vec{p}_{cT}^*/x_c)^2/s \simeq 0\,. \tag{3.3}$$

Now, because $s \gg p_{aT}^{*\,2}$, $p_{cT}^{*\,2}$, we get a relation

$$x_a \simeq x_c\,. \tag{3.4}$$

That is, in the case of forward scattering at $s \to \infty$, only the energy conservation $E_a^* = E_c^*$ is enough for the constraint $\hat{s} + \hat{t} + \hat{u} \simeq 0$. Finally, we have the simple relations

$$\hat{s} \simeq -\hat{u} \simeq x_a x_b s\,, \tag{3.5a}$$

$$\hat{t} \simeq -(\vec{p}_{aT}^* - \vec{p}_{cT}^*)^2\,. \tag{3.5b}$$

Next, we consider the decay process of c into hadron h in two-to-two scattering system. With the notation of Fig. 10, we have an expression

$$\hat{\vec{p}}_h = z_c \hat{\vec{p}}_c + \hat{\vec{k}}_{hT} \quad \text{with } \hat{\vec{p}}_c \cdot \hat{\vec{k}}_{hT} = 0\,, \tag{3.6}$$

where z_c is the scaling variable in the decay process $c \to h + X$, defined by $z_c = \hat{p}_{hL}/\hat{p}_c$. Projecting

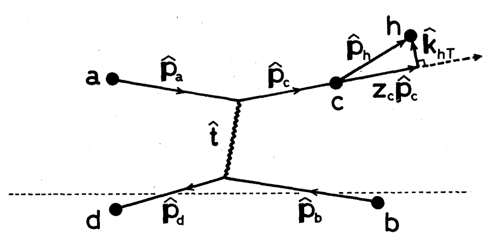

FIG. 10. Kinematics of subprocess $a + b \to c + d$ in two-to-two scattering system.

the vector $\hat{\vec{p}}_h$ into transversal and longitudinal components, we get

$$\hat{\vec{p}}_{hT} = z_c \hat{\vec{p}}_{cT} + (\hat{\vec{k}}_{hT})_T\,, \tag{3.7a}$$

$$\hat{p}_{hL} = z_c \hat{p}_{cL} + (\hat{\vec{k}}_{hT})_L\,. \tag{3.7b}$$

As discussed in Sec. II C, we are interested only in the quark (gluon) scattered in the forward region, so that we can put

$$(\hat{\vec{k}}_{hT})_T \simeq \hat{\vec{k}}_{hT} \text{ and } (\hat{\vec{k}}_{hT})_L \simeq 0\,, \tag{3.8}$$

that is,

$$\hat{\vec{p}}_{hT} \simeq z_c \hat{\vec{p}}_{cT} + \hat{\vec{k}}_{hT}\,, \tag{3.9a}$$

$$\hat{p}_{hL} \simeq z_c \hat{p}_{cL}\,. \tag{3.9b}$$

Now, as the Lorentz factor Γ of the two-to-two scattering system relative to c.m.s. is given by

$$\Gamma \simeq \frac{1}{2}\left[\left(\frac{x_b}{x_a}\right)^{1/2} + \left(\frac{x_a}{x_b}\right)^{1/2}\right], \tag{3.10}$$

we find

$$\hat{p}_{cL} \simeq \left(\frac{x_b}{x_a}\right)^{1/2} p_{cL}^* - \frac{1}{4}\left[\left(\frac{x_a}{x_b}\right)^{1/2} - \left(\frac{x_b}{x_a}\right)^{1/2}\right]\frac{(p_{cT}^*)^2}{(p_{cL}^*)^2}\,, \tag{3.11a}$$

$$\hat{p}_{hL} \simeq \left(\frac{x_b}{x_a}\right)^{1/2} p_{hL}^* - \frac{1}{4}\left[\left(\frac{x_a}{x_b}\right)^{1/2} - \left(\frac{x_b}{x_a}\right)^{1/2}\right]\frac{(p_{hT}^*)^2}{(p_{hL}^*)^2}\,. \tag{3.11b}$$

Because $(p_{c,hL}^*)^2 \gg (p_{c,hT}^*)^2$, we obtain

$$z_c \simeq \frac{\hat{p}_{hL}}{\hat{p}_{cL}} \simeq \frac{p_{hL}^*}{p_{cL}^*} \simeq \frac{z}{x_a} \quad \text{with } z = 2p_{hL}^*/\sqrt{s}\,. \tag{3.12}$$

One should keep in mind that the approximation used in the present subsection is of course not applicable for large-angle scattering.

B. Structure function $G(x, \vec{p}_T^*, Q^2)$ and decay function $D(z_c, \vec{k}_T^*, Q^2)$

Taking account of the parton transverse momentum $\vec{p}_{aT}^*$ inside the proton and of the scale-violation effect together, we write the structure function as

$$G_{a/A}(x_a, \vec{p}_{aT}^*, Q^2)dx_a d\vec{p}_{aT}^*$$
$$= G_{a/A}(x_a, Q^2)dx_a \psi(p_{aT}^{*\,2}/\langle p_T^2\rangle_{p\to q})d\vec{p}_{aT}^*/\pi\langle p_T^2\rangle_{p\to q}\,, \tag{3.13}$$

and choose $Q^2 = -\hat{t}$. Though the shape of $\psi(p_{aT}^{*\,2}/\langle p_T^2\rangle_{p\to q})$ may depend on the longitudinal scaling variable x_a as well as quark flavor, we assume it is independent of those and is expressed by the Gaussian form

$$\psi(p_{aT}^{*\,2}/\langle p_T^2\rangle_{p\to q}) = \exp(-p_{aT}^{*\,2}/\langle p_T^2\rangle_{p\to q}) \tag{3.14}$$

for the sake of simplicity. Explicit form of $G_{a/A}(x_a, Q^2)$ is discussed in Sec. IV A.

In a way similar to Eq. (3.13), taking account of hadron transverse momentum relative to the direction of quark (gluon) motion and of the scale-violation effect together, we write the decay function in the form

$$D_{h/c}(z_c, \vec{k}^*_{hT}, Q^2)dz_c\, d\vec{k}^*_{hT} = D_{h/c}(z_c, Q^2)dz_c\, \psi(k^{*\,2}_{hT}/\langle k_T^2\rangle_{q\to h})\, d\vec{k}^*_{hT}/\pi\langle k_T^2\rangle_{q\to h}, \tag{3.15}$$

where the form $\psi(k^{*\,2}_{hT}/\langle k_T^2\rangle_{q\to h})$ is of the same one as Eq. (3.14) after replacing the mean value $\langle p_T^2\rangle_{p\to q}$ into $\langle k_T^2\rangle_{q\to h}$, irrespective of z_c and constituent c. Explicit form of $D_{h/c}(z_c, Q^2)$ will also be given in Sec. IV A.

C. Cross section of subprocess $a + b \to c + d$

The cross section $d\hat{\sigma}(\hat{s}, \hat{t})/d\hat{t}$ for various subprocesses was recently calculated in the lowest order on the basis of QCD by Combridge, Kripfganz, and Ranft,[24] and independently by Cutler and Sivers.[25] The explicit forms of those are somewhat complicated for the purpose of deriving analytically the concerned cross section, and besides they depend on the types of subprocesses, $qq\to qq$, $qg\to qg$, and $gg\to gg$, and so on, where q and g denote quark and gluon, respectively. Fortunately, however, in the cosmic-ray energy region, we have a condition $\hat{s}$, $-\hat{u} \gg -\hat{t}$, good enough even in the region of extremely high momentum transfer $-\hat{t}\sim 100$ GeV$^2/c^2$. In such a case, we find a common simple form for any kind of subprocess, expressed as

$$\frac{d\hat{\sigma}}{d\hat{t}} \simeq T\,\frac{\pi\alpha_s^{\,2}(-\hat{t})}{\hat{t}^2}, \tag{3.16}$$

and only the numerical constant T depends on the type of subprocess,

$$T = \begin{cases} \frac{8}{9}, & \text{for } qq\to qq,\, q\bar{q}\to q\bar{q} \\ 0, & \text{for } \bar{q}q\to gg,\, gg\to q\bar{q} \\ 2, & \text{for } gq\to gq,\, \bar{q}g\to \bar{q}g \\ \frac{9}{2}, & \text{for } gg\to gg \end{cases} \tag{3.17}$$

which come mainly from color and spin averages over initial and final quarks (gluon). $\alpha_s(-\hat{t})$ is the effective quark-quark-gluon coupling constant, expected to have a form

$$\alpha_s(-\hat{t}) = \frac{12\pi}{27}\,\frac{1}{\ln(-\hat{t}/\Lambda^2)} \tag{3.18}$$

for three quark flavors u, d, and s. We put $\Lambda = 0.4$ GeV$/c$, the reasonable value estimated from deep-inelastic data.[26]

D. Invariant cross section of hadron

Invariant cross section of hadron h, produced through the hard scattering $a+b\to c+d$ and subsequent decay of c, is now written as

$$E^*_h \frac{d^3\sigma}{d\vec{p}^{*3}_h}(z, \vec{p}^*_{hT})\bigg|_{\substack{ab\to cd\\ c\to hX}} = \int\cdots\int [G_{a/A}(x_a, \vec{p}^*_{aT}, -\hat{t})dx_a d\vec{p}^*_{aT}][G_{b/B}(x_b, \vec{p}^*_{bT}, -\hat{t})dx_b d\vec{p}^*_{bT}]\left(\frac{1}{\pi}\frac{d\hat{\sigma}}{d\hat{t}}(\vec{p}^*_{cT})d\vec{p}^*_{cT}\right)_{ab\to cd} \times [D_{h/c}(z_c, \vec{k}^*_{hT}, -\hat{t})dz_c d\vec{k}^*_{hT}][\text{constraint factors}]. \tag{3.19}$$

Here, from Eqs. (3.9a) and (3.12),

$$[\text{constraint factors}] = z\,\delta(z - x_a z_c)\,\delta^{(2)}[\vec{p}^*_{hT} - (z_c\vec{p}^*_{cT} + \vec{k}^*_{hT})]. \tag{3.20}$$

Let us apply Mellin transformation from z to p, and Fourier transformation from $\vec{p}^*_{hT}$ to $\vec{q}$ simultaneously for Eq. (3.19),

$$\frac{1}{2\pi}\int_{-\infty}^{+\infty}\!\!\int d\vec{p}^*_{hT}\, e^{i\vec{q}\cdot\vec{p}^*_{hT}} \int_0^\infty dz\, z^{p-1} E^*_h \frac{d^3\sigma}{d\vec{p}^{*3}_h}(z, \vec{p}^*_{hT})\bigg|_{\substack{ab\to cd\\ c\to hX}} = \int_{Q_0^{\,2}}^\infty dQ^2 M_{a/A}(p, Q^2) N_{b/B}(Q^2)\,\frac{d\hat{\sigma}}{d\hat{t}}(Q^2)\bigg|_{ab\to cd} J_{h/c}(p, q, Q^2), \tag{3.21}$$

where

$$M_{a/A}(p, Q^2) = \int_0^1 dx_a\, x_a^{\,p} G_{a/A}(x_a, Q^2), \tag{3.22a}$$

$$N_{b/B}(Q^2) = \int_{x_{\min}}^1 dx_b G_{b/B}(x_b, Q^2), \tag{3.22b}$$

$$J_{h/c}(p, q, Q^2) = \frac{1}{2\pi}\int_0^1 dz_c\, z_c^{\,p} D_{h/c}(z_c, Q^2) \times J_0(z_c\, qQ)\, e^{-p_0^{\,2}(z_c)q^2/4}, \tag{3.22c}$$

with

$$p_0^{\,2}(z_c) = \langle k_T^2\rangle_{q\to h} + z_c^{\,2}\langle p_T^2\rangle_{p\to q}, \tag{3.22d}$$

and the lower limit of the integration with respect to Q^2 is discussed in Sec. IV A. $J_0(z_c qQ)$ in Eq. (3.22c) is a Bessel function with index 0.

We need the effective number of constituents in target nucleon $N_{b/B}$, which come mainly from "wee" partons, to estimate the production cross section of hadrons produced through forward hard scattering at $s\to\infty$. The lower limit $p^*_{\min}$ of effective parton momentum in the target nucleon is considered to be of the magnitude $\sim M_N$, the same order of magnitude with the "primordial" momentum of partons in nucleon. In the present paper, we choose $p^*_{\min}=1$ GeV/c, that is, $x_{\min}=2$ GeV/$\sqrt{s}$. The choice of $p^*_{\min}$, however, does not affect seriously the present calculations as long as it is not extremely small or large, because of logarithmic dependence of the effective number of partons $N_{b/B}$ on $p^*_{\min}$.

Applying the inverse Mellin transformation from p to z, and the inverse Fourier transformation from $\vec{q}$ to $\vec{p}^*_{hT}$ simultaneously for Eq. (3.21), we obtain

$$E^*_h \frac{d^3\sigma}{d\vec{p}_h^{*3}}(z,\vec{p}^*_{hT})\Big|_{\substack{ab\to cd\\ c\to hX}} = \int_z^1 dx\, \frac{z}{x}\,\Phi_h\Big(x,\frac{z}{x},p^*_{hT}\Big)\Big|_{\substack{ab\to cd\\ c\to hX}}, \tag{3.23}$$

where

$$\Phi_h(x,z_c,p^*_{hT})\Big|_{\substack{ab\to cd\\ c\to hX}} = \int_{Q_0^2}^{\infty} dQ^2\, \frac{\pi\alpha_s^2(Q^2)}{Q^4} S(z_c,p^*_{hT},Q^2)\Lambda_h(x,z_c,Q^2)\Big|_{\substack{ab\to cd\\ c\to hX}}, \tag{3.24}$$

$$S(z_c,p^*_{hT},Q^2)=\frac{1}{\pi p_0^2(z_c)}e^{-(p^{*2}_{hT}+z_c^2Q^2)/p_0^2(z_c)}I_0\Big(\frac{2z_cQp^*_{hT}}{p_0^2(z_c)}\Big), \tag{3.25}$$

and

$$\Lambda_h(x,z_c,Q^2)\big|_{\substack{ab\to cd\\ c\to hX}}=[G_{a/A}(x,Q^2)T_{ab\to cd}N_{b/B}(Q^2)]D_{h/c}(z_c,Q^2)\ . \tag{3.26}$$

$I_0(y)$ appearing in Eq. (3.25) denotes the modified Bessel function with index 0, and $T_{ab\to cd}$ in Eq. (3.26) the weight factor for the subprocess $a+b\to c+d$ as summarized in Eq. (3.17). $S(z_c,p^*_{hT},Q^2)$ corresponds to so-called smearing effects due to the transverse momenta $(\vec{p}_T)_{p\to q}$ and $(\vec{k}_T)_{q\to h}$. In the limit of $\langle p_T^2\rangle_{p\to q}\to 0$ and $\langle k_T^2\rangle_{q\to h}\to 0$ (no smearing case), Eq. (3.25) leads to a natural result,

$$S(z_c,p^*_{hT},Q^2)=\frac{1}{\pi}\,\delta(p^{*2}_{hT}-z_c^2Q^2)\ . \tag{3.27}$$

Until now, we have restricted ourselves to the special case that hadron h is produced through the subprocess $a+b\to c+d$ and subsequent decay of c into h. It is an easy task to generalize the above procedure, including all subprocesses.

Let us consider seven constitutents (u, d, s, $\bar{u}$, $\bar{d}$, $\bar{s}$, gluon) and define the following matrices:

$$G_A(x,Q^2)=\begin{bmatrix}u_A\\ d_A\\ s_A\\ \bar{u}_A\\ \bar{d}_A\\ \bar{s}_A\\ g_A\end{bmatrix},\quad N_B(Q^2)=\begin{bmatrix}n_{u/B}\\ n_{d/B}\\ n_{s/B}\\ n_{\bar{u}/B}\\ n_{\bar{d}/B}\\ n_{\bar{s}/B}\\ n_{g/B}\end{bmatrix},\quad \text{and } D_h(z_c,Q^2)=\begin{bmatrix}D_{u\to h}\\ D_{d\to h}\\ D_{s\to h}\\ D_{\bar{u}\to h}\\ D_{\bar{d}\to h}\\ D_{\bar{s}\to h}\\ D_{g\to h}\end{bmatrix}, \tag{3.28}$$

and recalling Eq. (3.17),

$$T=\begin{bmatrix}\frac{8}{9}, & \ldots, & \frac{8}{9}, & 2\\ \vdots & \ddots & \vdots & \vdots\\ \frac{8}{9}, & \ldots, & \frac{8}{9}, & 2\\ 2, & \ldots, & 2, & \frac{9}{2}\end{bmatrix}. \tag{3.29}$$

Then Eq. (3.26) is modified as follows:

$$\begin{aligned}\Lambda_h(x,z_c,Q^2)&=[G_A(x,Q^2)TN_B(Q^2)]^*D_h(z_c,Q^2)\\ &=[\tfrac{8}{9}(u_AD_{u\to h}+d_AD_{d\to h}+s_AD_{s\to h}+\bar{u}_AD_{\bar{u}\to h}+\bar{d}_AD_{\bar{d}\to h}+\bar{s}_AD_{\bar{s}\to h})+2g_AD_{g\to h}]n_{g/B}+\tfrac{9}{2}g_AD_{g\to h}n_{g/B}\,,\end{aligned} \tag{3.30a}$$

with

$$n_{q/B}=n_{u/B}+n_{d/B}+n_{s/B}+n_{\bar{u}/B}+n_{\bar{d}/B}+n_{\bar{s}/B}\,. \tag{3.30b}$$

Here, [ ]* in Eq. (3.30a) denotes the transposed matrix.

Since the variable z is approximately equal to the fractional energy E_h/E_0 defined in LS for the region $\theta^* \lesssim 20°$ and $\sqrt{s}\gg M_N$, we finally have a general formula for the production cross section of hadrons produced by forward hard scattering in LS, including the smearing effect

$$E_h\frac{d^3\sigma}{d\vec{p}_h^{\,3}}=\int_z^1 dx\,\frac{z}{x}\,\Phi_h\left(x,\,\frac{z}{x},p_{hT}\right),$$

with

$$z=2p^*_{hL}/\sqrt{s}\simeq E_h/E_0\,. \tag{3.31}$$

In the case of no smearing, we get a simple result, with use of the relation (3.27),

$$E_h\frac{d^3\sigma}{d\vec{p}_h^{\,3}}=p_{hT}^{-4}\int_z^{z_0}dx\left(\frac{z}{x}\right)^3\alpha_s^2(Q^2)\Lambda_h\left(x,\,\frac{z}{x},\,Q^2\right),$$

with

$$Q^2=\left(\frac{x}{z}\right)^2p_{hT}^{\,2}\,, \tag{3.32a}$$

where

$$z_0=\begin{cases}1 & \text{for } p_{hT}\geq Q_0\,,\\ p_{hT}/Q_0 & \text{for } p_{hT}<Q_0\,,\end{cases} \tag{3.32b}$$

showing approximate p_{hT}^{-4} behavior as expected, because of weak dependence of α_s and Λ_h on Q^2.

Equation (3.31) is represented also by the complex integral form, with use of Eq. (3.21),

$$E_h\frac{d^3\sigma}{d\vec{p}_h^{\,3}}=\frac{1}{2\pi i}\int_C dp\,z^{-p}M_\Phi(p,p_{hT})\,, \tag{3.34}$$

where

$$M_\Phi(p,p_{hT})=\int_{Q_0^2}^\infty\frac{\pi\alpha_s^2(Q^2)}{Q^4}[M_A(p,Q^2)TN_B(Q^2)]^*\times M_D(p,p_{hT},Q^2)\,, \tag{3.35}$$

with

$$M_D(p,p_{hT},Q^2)=\int_0^1 dz_c z_c^{\,p}D_h(z_c,Q^2)S(z_c,p_{hT},Q^2)\,,$$

and integral path C is running in the convergency domain parallel to the imaginary axis.

E. γ-ray production cross section

Now, we can estimate the production cross section of π^0 from Eq. (3.31). The work we must do here concerns the decay process of $\pi^0\to 2\gamma$, as we detect γ rays in the C-jet data.

Generally, it is somewhat troublesome to consider such processes in a three-dimensional way. Fortunately, however, the magnitude of the transverse momentum of γ ray relative to the direction of π^0 motion is given by

$$p_{T\gamma}^{(\text{decay})}\simeq m_{\pi^0}[v(1-v)]^{1/2}\lesssim 70\text{ MeV}/c\,,$$

with

$$v=E_\gamma/E_{\pi^0}\,. \tag{3.36}$$

Here m_{π^0} is the mass of π^0, and E_γ, E_{π^0} are energies of γ ray and π^0, respectively. The value 70 MeV/c in the above is much smaller than those of interest now, $\gtrsim$500 MeV/c. Then, neglecting the deflection of γ ray caused by the decay of π^0 moving with the transverse momentum $\vec{p}_{T\pi^0}$, the transverse momentum $\vec{p}_{T\gamma}$ of γ ray is given by

$$\vec{p}_{T\gamma}\simeq v\vec{p}_{T\pi^0}\,. \tag{3.37}$$

So, we have the following distribution function for the process concerned:

$$\xi(\vec{p}_{\pi^0},\vec{p}_\gamma)\,\frac{d\vec{p}_\gamma^{\,3}}{E_\gamma}=2\delta^{(2)}(\vec{p}_{T\gamma}-v\vec{p}_{T\pi^0})dv\,d\vec{p}_{T\gamma}\,. \tag{3.38}$$

Finally, combining Eq. (3.31) with Eq. (3.38), we obtain the production cross section of γ ray

$$E_\gamma\frac{d^3\sigma}{d\vec{p}_\gamma^{\,3}}=\iint E_{\pi^0}\frac{d^3\sigma}{d\vec{p}_{\pi^0}^{\,3}}\,\xi(\vec{p}_{\pi^0},\vec{p}_\gamma)\,\frac{d\vec{p}_{\pi^0}^{\,3}}{E_{\pi^0}}$$
$$=\frac{2}{z_\gamma}\int_{z_\gamma}^1 z\,dz\int_z^1\Phi_{\pi^0}\left(x,\,\frac{z}{x},\,\frac{z}{z_\gamma}p_{T\gamma}\right)\frac{dx}{x}\,, \tag{3.39}$$

with

$$z_\gamma=2p^*_{\gamma L}/\sqrt{s}\simeq k_\gamma E_\gamma/\textstyle\sum E_\gamma\,.$$

In the case of no smearing, with use of Eq. (3.27), we find

$$E_\gamma\frac{d^3\sigma}{d\vec{p}_\gamma^{\,3}}=2p_{T\gamma}^{-4}\int_{z_\gamma}^{z_0}\frac{dz}{z}\int_z^{z_0}dx\left(\frac{z_\gamma}{x}\right)^3\times\alpha_s^2(Q^2)\Lambda_{\pi^0}\left(x,\,\frac{z}{x},\,Q^2\right), \tag{3.40}$$

with

$$Q^2=\frac{x^2}{z_\gamma^{\,2}}p_{T\gamma}^{\,2}\,,$$

and z_0 is the same one as given by Eq. (3.32b) after replacing p_{hT} into $p_{T\gamma}$. Equation (3.40) gives approximate $p_{T\gamma}^{-4}$ behavior, similarly as in the case of Eq. (3.32a).

IV. NUMERICAL CALCULATIONS AND COMPARISON WITH EXPERIMENTAL DATA

A. Explicit parametrizations for $G_p(x,Q^2)$ and $D_{\pi^0}(z_c,Q^2)$

In Sec. III we derived analytically the invariant production cross section of hadron and γ ray. We introduced there a cutoff parameter Q_0^2 as found in Eq. (3.21), which was introduced, for convenience, to eliminate the divergence in the integrand at $Q^2 \to 0$. Now, the value Q_0^2 is nothing but the boundary condition for renormalization-group equation to obtain structure function $G(x, Q^2)$ and decay function $D(z_c, Q^2)$ at any other Q^2. Of course, Q_0^2 is chosen arbitrarily, but must be large enough, at least $Q_0^2 \gtrsim M_N^2$, so that the coupling constant $\alpha_s(Q^2)$ is small. That is, Q_0^2 is the lower limit applicable for the quark-parton picture in the concerned process.

As presented in many papers,[26] the solution of renormalization-group equation for $G(x, Q^2)$ is expressed in the form of its Mellin transformation $M(p, Q^2)$, just the same function as defined by Eq. (3.22a),

$$M(p, Q^2) = R(p, Q^2, Q_0^2) M(p, Q_0^2) . \tag{4.1}$$

Here, $R(p, Q^2, Q_0^2)$ is a 7×7 matrix, corresponding to seven constituents ($u, d, s, \bar{u}, \bar{d}, \bar{s}$, gluon), and of course unit matrix at $Q^2 = Q_0^2$. Explicit form of R is summarized, for example, in Ref. 26. Substituting Eq. (4.1) into Eq. (3.35), and performing complex integration with respect to p, we can obtain the cross section concerned. The form R is, however, slightly complicated for our purpose, so in the present paper, we assume an empirical form for $G(x, Q^2)$ so as to fit the experimental data.

Recalling that the form of R_{ij} is expanded as[26]

$$R_{ij}(p, Q^2, Q_0^2) \simeq \delta_{ij} + N_{ij}(p, Q_0^2) \ln(Q^2/Q_0^2) , \tag{4.2}$$

in the neighborhood of $Q^2 \sim Q_0^2$, it may be reasonable to choose

$$G_p(x, Q^2) = G_p(x, Q_0^2) e^{-\beta(x) \ln Q^2/Q_0^2} . \tag{4.3}$$

Here $G_p(x, Q_0^2)$ and $\beta(x)$ are determined from deep-inelastic data. In the present paper, we set $Q_0^2 = 2\ \mathrm{GeV}^2/c^2$, above which Eq. (3.16), derived from the perturbation theory, makes sense.

Feynman and Field (hereafter called FF)[5] determined phenomenologically distribution functions of quarks inside the proton $q^{\mathrm{FF}}(x)$ ($q = u, d, s, \bar{u}, \bar{d}, \bar{s}$), neglecting the scale violation, on the basis of e-p and μ-p deep-inelastic data. Here, we modify slightly their parametrization,

$$G_p(x, Q_0^2)\big|_{\mathrm{quarks}} = q^{\mathrm{FF}}(x)\, e^{\alpha(x)} . \tag{4.4}$$

Here, $q^{\mathrm{FF}}(x)$ denotes six-component vector, each with u^{FF}, d^{FF}, s^{FF}, $\bar{u}^{\mathrm{FF}}$, $\bar{d}^{\mathrm{FF}}$, and $\bar{s}^{\mathrm{FF}}$. The small correction term $\alpha(x)$ is determined from the experimental data on x distribution at $Q^2 = Q_0^2$.

In the present stage, unfortunately, we have no experimental information to determine the shape of the structure function of gluon; instead we know only that its mean momentum fraction $\langle x \rangle \sim 0.5$. So, we assume the following shape suggested by the dimensional-counting rule at $x \to 1$[6]:

$$x g^{\mathrm{DC}}(x) = 3(1-x)^5 . \tag{4.5}$$

Finally, we have the following form for $G_p(x, Q^2)$ in the matrix representation:

$$G_p(x, Q^2) \equiv \begin{pmatrix} q(x, Q^2) \\ g(x, Q^2) \end{pmatrix} = \begin{pmatrix} q^{\mathrm{FF}}(x) \\ g^{\mathrm{DC}}(x) \end{pmatrix} e^{\alpha(x)+\beta(x)\ln(Q^2/Q_0^2)} . \tag{4.6}$$

Though the functional forms of α and β may differ among quark flavors, in particular between quark and gluon, we assume them to be independent of flavor for the sake of simplicity.

With use of the well-known relation for e-p and μ-p collisions,[27]

$$\nu W_2^{(ep)}(x, Q^2) = \tfrac{4}{9} x(u+\bar{u}) + \tfrac{1}{9} x(d+\bar{d}+s+\bar{s}) , \tag{4.7}$$

we choose

$$\alpha(x) = 2.1x^2 - 0.13x + 0.83\sqrt{x} - 0.34\sqrt[4]{x} - 0.083 , \tag{4.8a}$$

$$\beta(x) = 0.19x - 1.2\sqrt{x} + 0.49\sqrt[4]{x} + 0.12 . \tag{4.8b}$$

In Fig. 11(a), we demonstrate the experimental data[9] on x distribution at several values of Q^2, together with empirical curves expected from Eqs. (4.6) and (4.8). While in Fig. 11(b), we present the data[28] on Q^2 dependence of $\nu W_2^{(ep)}(x, Q^2)$ at several fixed values of x. Both figures tell us that the present empirical formula (4.6) reproduces well the deep-inelastic data exhibiting scale violation over wide ranges of x and Q^2.

Momentum fraction of quarks (gluon) inside proton, obtained by Eqs. (4.6) and (4.8), is now slightly different from those estimated by FF[5] as shown in Fig. 12. One finds both momentum fractions of quark and gluon depend weakly on Q^2, lying around 0.5, although momentum conservation, $\langle x \rangle_{\mathrm{quark}} + \langle x \rangle_{\mathrm{gluon}} = 1$, is a little bit broken. The trivial break of the momentum conservation does not, however, yield any serious effect on the present calculations.

In Figs. 13(a) and 13(b), we compared our empirical formulas on $\nu W_2^{(ep)}(x, Q^2)$ and $xg(x, Q^2)$ with those expected from QCD calculation presented in Ref. 7. One sees the present parametrization for $G_p(x, Q^2)$ is not inconsistent with QCD prediction.

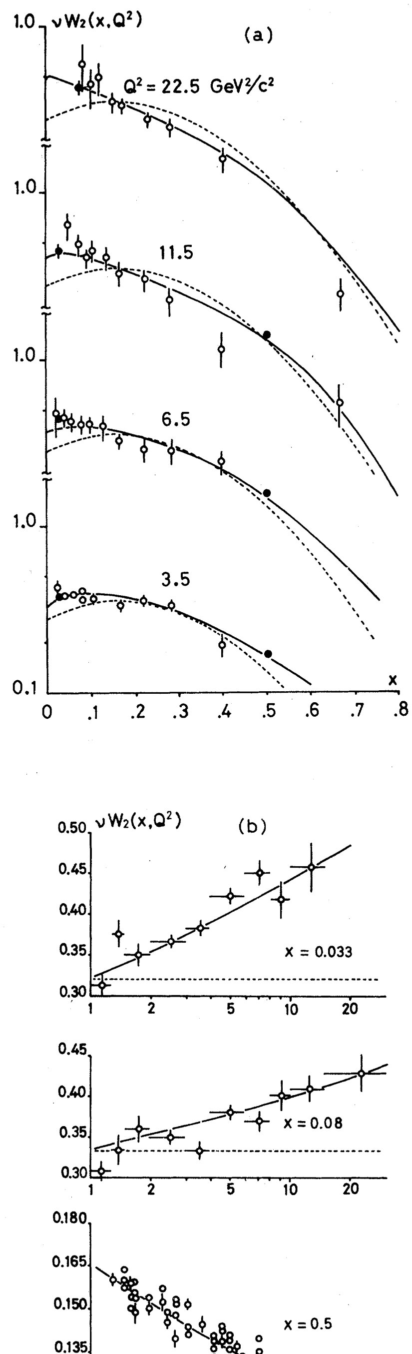

FIG. 11. $\nu W_2(x, Q^2)$ distributions versus x with fixed Q^2 (a), and versus Q^2 with fixed x (b). The data in the former are from Refs. 9 (open circle) and 28 (black circle). The data in the latter are from Ref. 28. Solid curves in both figures are those obtained from the present parametrization (4.6), while dashed ones from Ref. 5 neglecting scale violation.

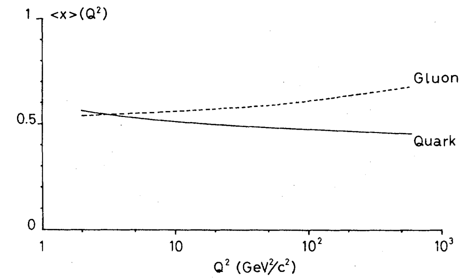

FIG. 12. Momentum fraction of quarks (solid curve) and gluons (dashed one) inside proton versus Q^2.

Next, we discuss the decay function $D_h(z_c, Q^2)$ including scale-violation effect. In C-jet data, we observe γ-ray components mainly from neutral pion decay $\pi^0 \to 2\gamma$. So, we consider the decay function $D_{\pi^0}(z_c, Q^2)$ of quarks (gluon) into π^0 only. Here, we observe both π^0's produced directly through quark (gluon) decay and indirectly via subprocess quark (gluon) $\to$ vector meson $\to \pi^0$. Therefore, the decay function $D_{\pi^0}(z_c, Q^2)$ must be total net one including both π^0's.

Now, similarly as in the case of structure function $G_p(x, Q^2)$, we assume that the decay function, taking into account the scale-violation effect, is expressed as

$$D_{\pi^0}(z_c, Q^2) \equiv \begin{pmatrix} D_{q\to\pi^0}(z_c, Q^2) \\ D_{g\to\pi^0}(z_c, Q^2) \end{pmatrix} = \begin{pmatrix} D^{\mathrm{FF}}_{q\to\pi^0}(z_c) \\ D^{\mathrm{DC}}_{g\to\pi^0}(z_c) \end{pmatrix} e^{\tilde{\alpha}(z_c)+\tilde{\beta}(z_c)\ln(Q^2/Q_0^2)} . \tag{4.9}$$

Here $D^{\mathrm{FF}}_{q\to\pi^0}(z_c)$ denotes six-component vector, each parametrized by FF,[5] which includes both π^0's due to direct and indirect decays of quarks. The decay function of gluon into π^0 is given by

$$z_c D^{\mathrm{DC}}_{g\to\pi^0}(z_c) = \tfrac{4}{5}(1-z_c)^3 , \tag{4.10}$$

as suggested by dimensional-counting rule at $z_c \to 1$.[6,25] The factor $\frac{4}{5}$ comes from the fact that 60% (Ref. 5) of momentum is carried by pions (direct + indirect) when decaying from a parent quark, and then ~20% of momentum will be released into π^0 because the parent gluon is a flavor isosinglet.

Unfortunately, in the present stage, the data on $D_{\pi^0}(z_c, Q^2)$ including scale violation are too poor, particularly at large Q^2, to determine the correction terms $\tilde{\alpha}(z_c)$ and $\tilde{\beta}(z_c)$. Here, we assume they are similar to those shown in Eqs. (4.8a) and (4.8b),

$$\tilde{\alpha}(z_c) = 0.7 z_c^2 - 0.13 z_c + 0.83\sqrt{z_c} - 0.34\sqrt[4]{z_c} - 0.083 , \tag{4.11a}$$

$$\tilde{\beta}(z_c) = \beta(z_c) . \tag{4.11b}$$

In Figs. 14(a) and 14(b), we show the decay

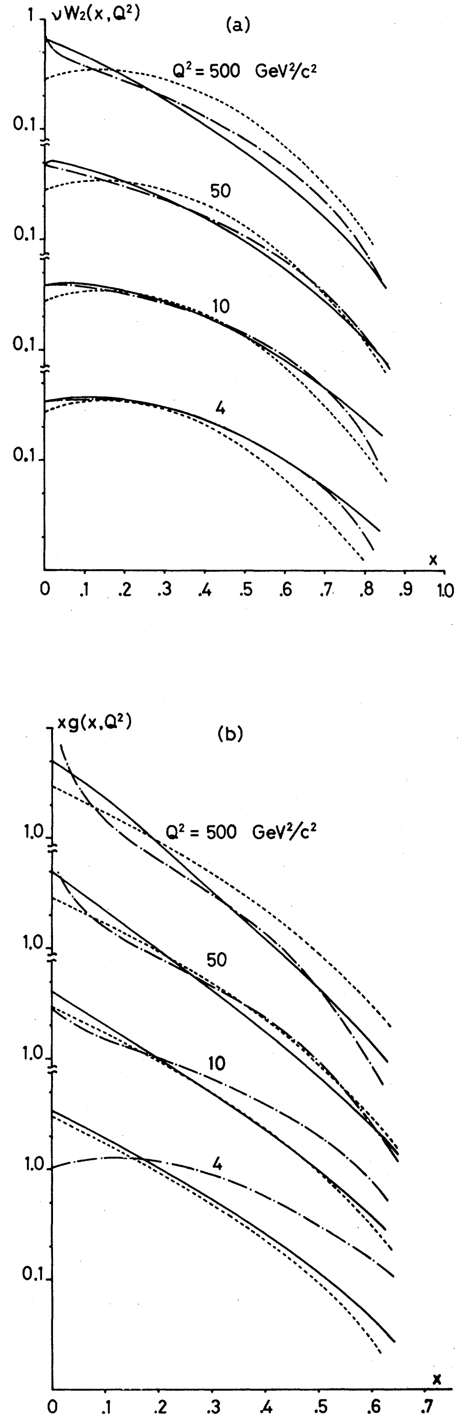

FIG. 13. Comparison with the present empirical formula (solid curves) on $\nu W_2(x,Q^2)$ (a) and $xg(x)$ (b) at various Q^2's with those presented in Ref. 5 (dashed ones), and with those in Ref. 7 (dash-dotted ones). The curves from Ref. 5 (dashed ones) are always independent of Q^2, because of neglecting scale violation.

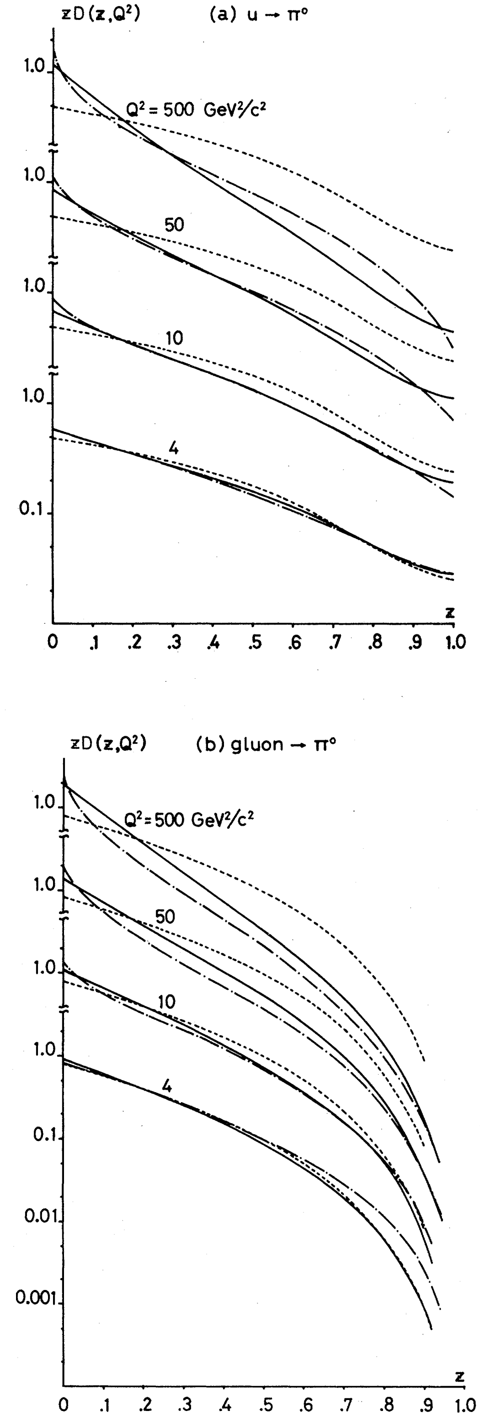

FIG. 14. Comparison of the decay functions (a) for $u \to \pi^0$ and (b) for gluon $\to \pi^0$. The present empirical formula (4.9) (solid curves), the one from Ref. 5 (dashed ones), and the one from Ref. 7 (dashed ones) are shown at various Q^2's.

functions at several sets of Q^2 for the processes $u\to\pi^0$ and gluon $\to\pi^0$ thus obtained, together with the QCD calculation shown in Ref. 7. The latter, of course, includes π^0's produced indirectly through the decay of vector meson. Both figures tell us that our parametrization is in agreement with the QCD calculation in the wide range of Q^2.

B. Production cross section of π^+ and K^+ at $\sqrt{s} = 540$ GeV

Although it is hard to get the production cross section of π^+ and K^+ through cosmic-ray-beam interaction, it seems meaningful for the forthcoming giant machine, for instance p-$\bar{p}$ collision with $\sqrt{s} = 540$ GeV,[29] which will be operated at Fermilab and CERN in the early 1980's. So, we consider here a case wherein the proton is moving to the right (forward direction) and the antiproton to the left (backward direction).

In order to calculate the cross section of π^+ (K^+) with use of Eq. (3.31), we need to know the decay functions of quark and gluon into π^+ (K^+). Here, we use again the parametrization obtained by FF[5] for the decay of quark into π^+ (K^+), and the one expected from the dimensional-counting rule[6,25] for the decay of gluon into π^+ (K^+),

$$z_c D^{\mathrm{DC}}_{g\to\pi^+}(z_c) = \tfrac{4}{5}(1-z_c)^3 \text{ and } z_c D^{\mathrm{DC}}_{g\to K^+}(z_c) = \tfrac{2}{5}(1-z_c)^3 . \tag{4.12}$$

In Figs. 15(a) and 15(b), we show p_T distributions of π^+ and K^+, produced in the forward cone $\theta^* \lesssim 20°$, at various values of z in three cases for smearing effects. One finds the smearing effect is more significant in the region $p_T = 2 \sim 7$ GeV/c as z increases.

It may be interesting to see the above cross section in the backward cone $\theta^* \gtrsim 160°$. We demonstrate the numerical results in Figs. 16(a) and 16(b), together with those observed in the forward cone. One finds that as z increases the difference between the above two becomes more significant; for instance, the production cross section of π^+ at $z = 0.5$ in the backward cone is expected to be ~40% of that in the forward cone. This is natural since the decay probability of quark into π^+ (K^+) is larger than that of antiquark into π^+ (K^+), and in addition, the contribution of gluon becomes smaller than quark and antiquark as $z\to 1$.

Figures 17(a) and 17(b) present z distributions of π^+ and K^+, respectively, both together with those expected in the backward cone.

C. Numerical results on transverse-momentum distribution of γ rays at C-jet energy region

In Fig. 18, we show the numerical results on the production cross section of γ ray at C-jet energy

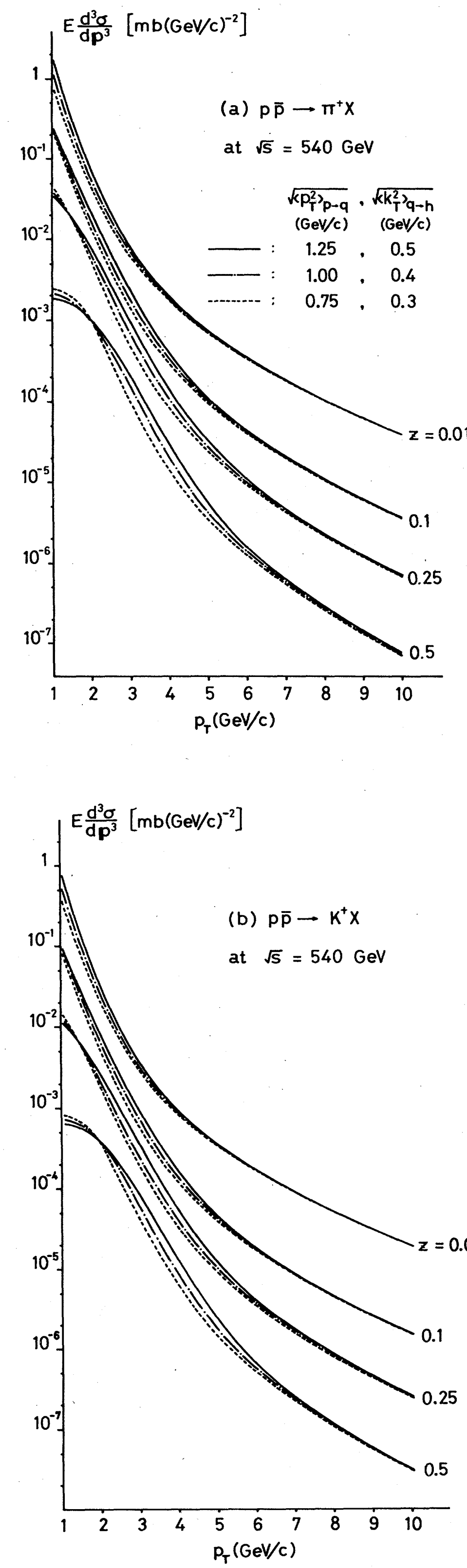

FIG. 15. p_T distributions of π^+ (a) and K^+ (b) at $\sqrt{s} = 540$ GeV in $p\bar{p}$ collision.

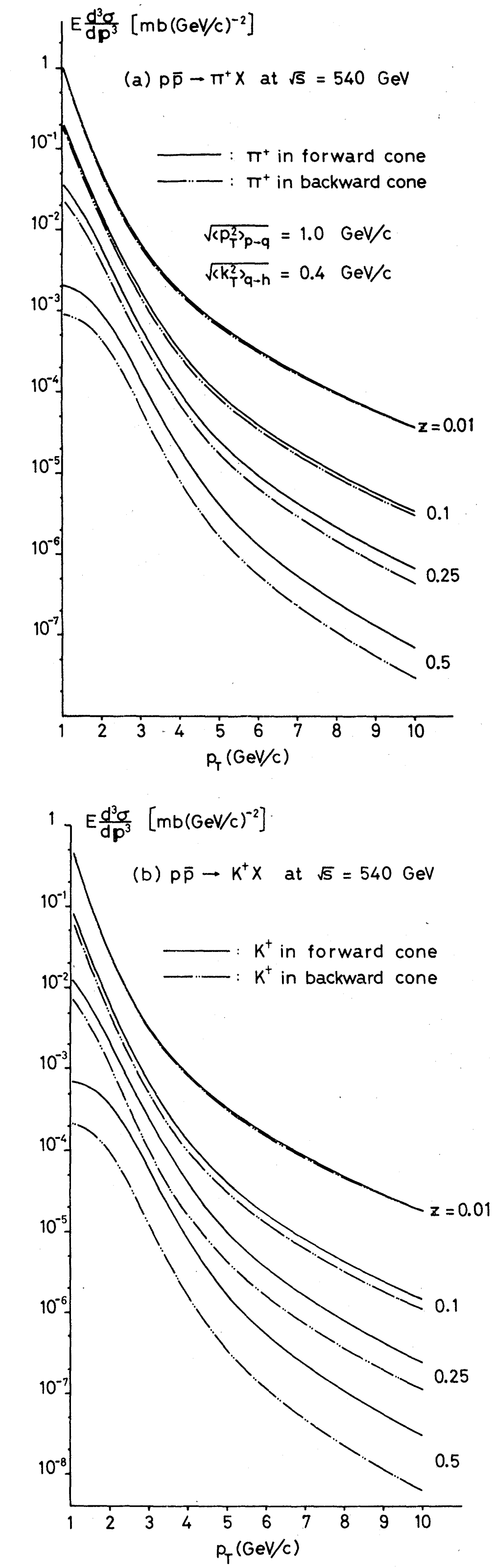

FIG. 16. Comparison of p_T distributions of π^+ (a) and K^+ (b) produced in the forward cone with those in the backward cone in $p\bar{p}$ collision.

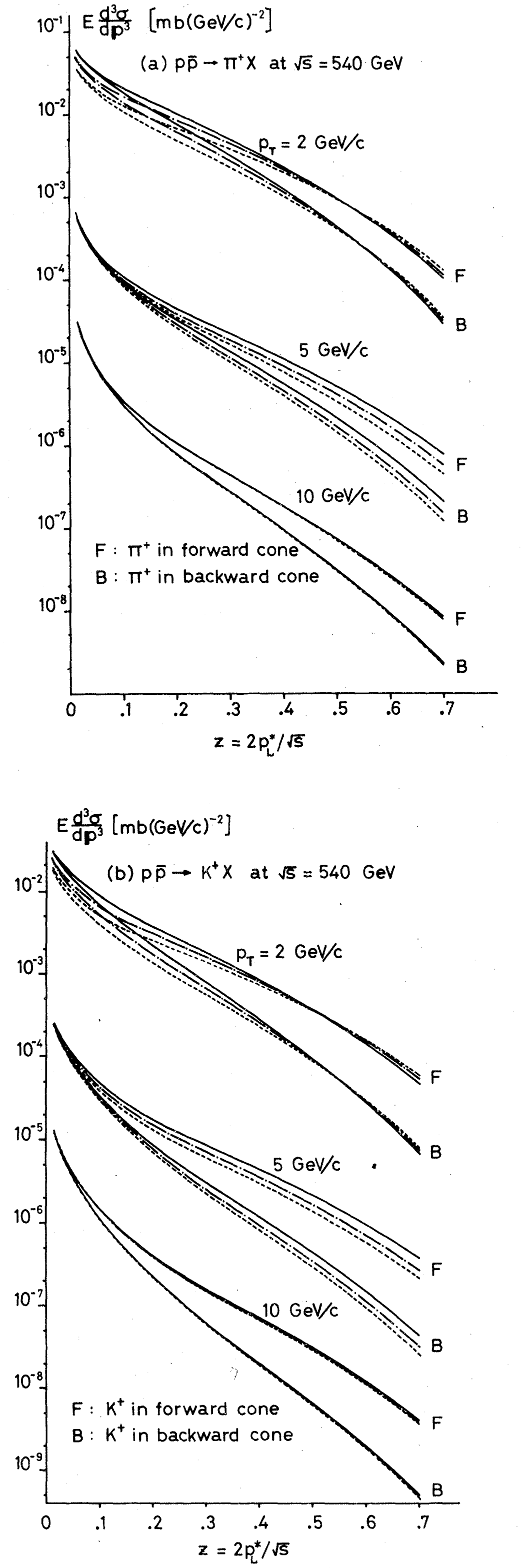

FIG. 17. z distributions of π^+ (a) and K^+ (b) at $\sqrt{s} = 540$ GeV in $p\bar{p}$ collision. The distinctions among solid, dash, and dash-dotted curves are the same as in Fig. 15 (a).

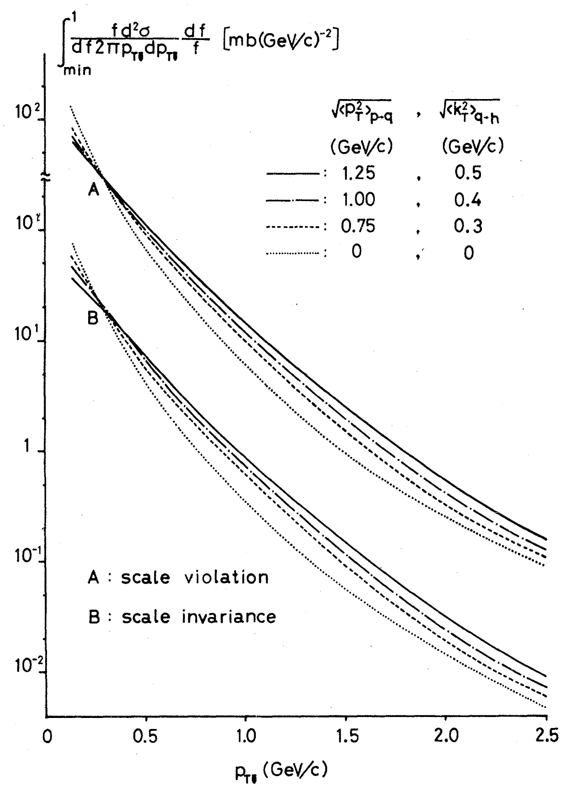

FIG. 18. Theoretical curves on $p_{T\gamma}$ distribution at C-jet energy region $\sqrt{s} = 523$ GeV, integrated over f ($= z_\gamma / \langle k_\gamma \rangle_{\text{bias}}$) from 0.025 to 1.

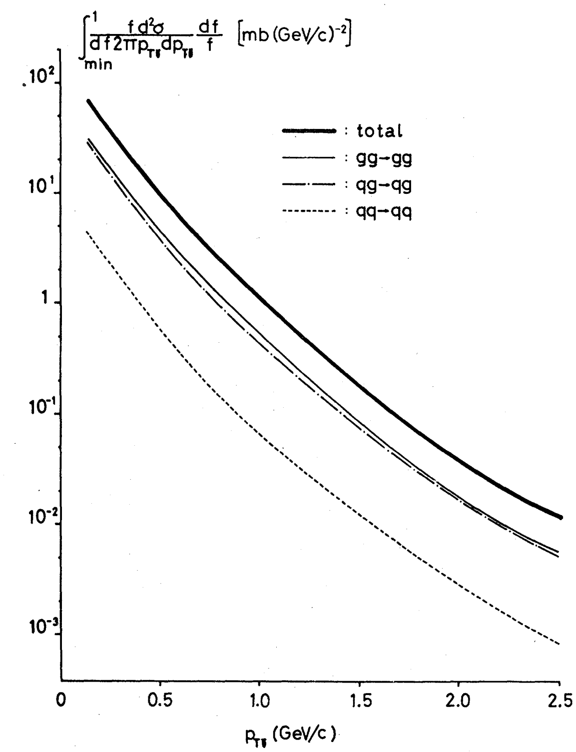

FIG. 19. Partial production cross sections of γ rays with $f \geqslant 0.025$ at $\sqrt{s} = 523$ GeV, originated in three kinds of subprocesses $q+q \to q+q$, $q+g \to q+g$, and $g+g \to g+g$, together with the superposed total one, in the case of $(\langle p_T{}^2\rangle_{p\to q})^{1/2} = 1$ GeV/c and $(\langle k_T{}^2\rangle_{q\to h})^{1/2} = 0.4$ GeV/c.

region ($\sqrt{s} = 523$ GeV), integrated over f from 0.025 to 1. Two cases of the cross sections, the scale violation (A) and the scale invariance (B), are compared. The lower limit 0.025 for f corresponds to 0.007 for $z_{\gamma\,\min}$, assuming $\langle k_\gamma \rangle_{\text{bias}} = 0.28$ in Eq. (2.9). In the case of the calculation for scale invariance, we used the structure function and the decay function omitting the exponential terms in Eqs. (4.6) and (4.9).

We present in Fig. 18 several sets of values for $(\langle p_T{}^2\rangle_{p\to q})^{1/2}$ and $(\langle k_T{}^2\rangle_{q\to h})^{1/2}$ together. One finds that the set $(\langle p_T{}^2\rangle_{p\to q})^{1/2} = 1.25$ GeV/c and $(\langle k_T{}^2\rangle_{q\to h})^{1/2} = 0.5$ GeV/c yields higher cross section by nearly three times more than the no-smearing case in the region $p_{T\gamma} = 1$–2 GeV/c, for both the cases of scale violation and scale invariance. One sees also that the cross section in the case of scale violation is approximately twice that in the case of scale invariance over all ranges in $p_{T\gamma}$.

In Fig. 19, we show separately the cross sections of γ rays originated in the subprocesses $qq \to qq$, $qg \to qg$, and $gg \to gg$ for the set $(\langle p_T{}^2\rangle_{p\to q})^{1/2} = 1$ GeV/c and $(\langle k_T{}^2\rangle_{q\to h})^{1/2} = 0.4$ GeV/c, to see which kind of subprocess is the most effective. One finds that the gluon plays the dominant role in the forward hard scattering at cosmic-ray energy region $\sqrt{s} \sim 500$ GeV.

In Fig. 20, we show the dependence on $Q_0{}^2$, the cutoff momentum transfer of the production cross section of γ ray at $(\langle p_T{}^2\rangle_{p\to q})^{1/2} = 1$ GeV/c and

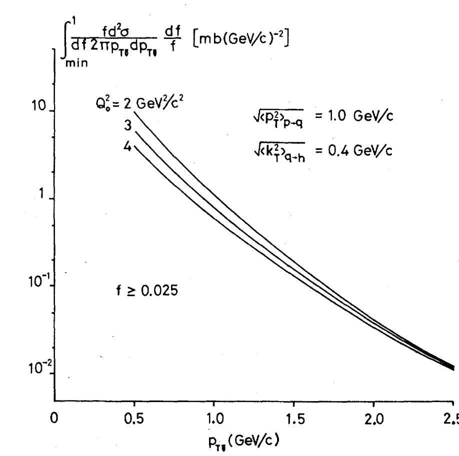

FIG. 20. Dependence of the production cross section of γ ray with $f \geqslant 0.025$ on $Q_0{}^2$, the cutoff momentum transfer, in the case of $(\langle p_T{}^2\rangle_{p\to q})^{1/2} = 1$ GeV/c and $(\langle k_T{}^2\rangle_{q\to h})^{1/2} = 0.4$ GeV/c.

$(\langle k_T{}^2\rangle_{q\to h})^{1/2}=0.4$ GeV/c, integrated over f from 0.025 to 1. In the region $p_{T\gamma}\lesssim 1.5$ GeV/c, the difference between the sets of $Q_0{}^2=2$ and 4 GeV^2/c^2 seems significant.

D. Comparison with emulsion-chamber data

In Fig. 3, we showed $p_{T\gamma}$ distribution per interaction, obtained by two-story EC at Mt. Chacaltaya. To compare it with the theoretical calculations presented in Fig. 18, we need to know σ_{inel} as well as the bias factor B. Although we have no direct information on the magnitude of σ_{inel} at ultrahigh-energy region $E_0 \gtrsim 10^{14}$ eV, we expect $\sigma_{\text{inel}}=35\sim 45$ mb in relevant energy range, through the investigation[30] on the attenuation of high-energy cosmic-ray particles. Various theoretical considerations[31] also give nearly the same magnitude. So, in the present paper, we assume $\sigma_{\text{inel}}=40$ mb. As for the bias factor B, we put $B=1.68$ corresponding to the choice $\langle k_\gamma\rangle_{\text{bias}}=0.28$. Finally, in Fig. 21, we show the production cross section of γ ray in the absolute form, together with the theoretical curves.

The theoretical curves expected from the hard scattering are in surprisingly nice agreement with the net C-jet data after subtracting the contribution of background soft γ rays not only in the shape, but also in the absolute value. Although it seems difficult in this stage to say which choice of $(\langle p_T{}^2\rangle_{p\to q})^{1/2}$ and $(\langle k_T{}^2\rangle_{q\to h})^{1/2}$ is the best one, we can conclude definitely that neither the case of the scale invariance nor the no-smearing case are compatible with the C-jet data with the energy region $\sqrt{s}\sim 500$ GeV.

Next let us show f $(=z_\gamma/\langle k_\gamma\rangle_{\text{bias}})$ distributions with $p_{T\gamma}\geqslant 750$ MeV/c and $\geqslant 850$ MeV/c in Fig. 22 drawn in the form of absolute cross section, assuming $\sigma_{\text{inel}}=40$ mb and $B=1.68$. The theoretical curves are also demonstrated there, which are calculated on the basis of the formula (3.39). The fall of the experimental points in the region of $f\lesssim 0.02$ is merely due to the effect of the detection loss. Again we find satisfactory agreement with each other, taking the contributions of the background soft γ rays into account.

V. CONCLUDING REMARKS

Although there remain several ambiguities on the choices of free parameters B, p^*_{min} and $Q_0{}^2$, and also on the background subtraction of γ rays

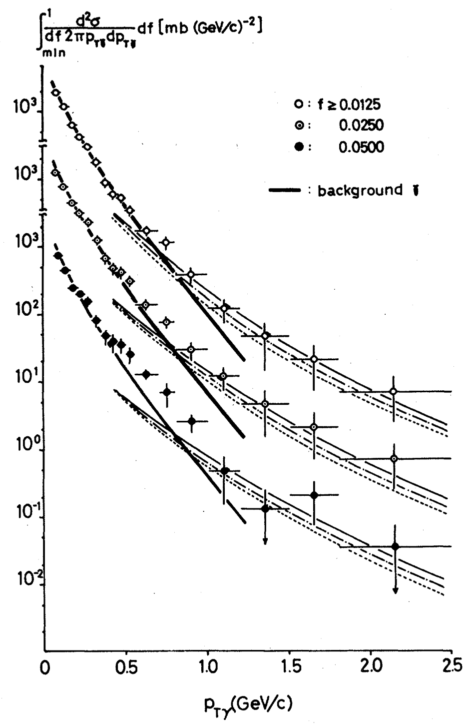

FIG. 21. Comparison of $p_{T\gamma}$ distribution between the C-jet data and the theoretical calculations. Three kinds of curves are the same as those in the case of scale violation (A) shown in Fig. 18. Background curves (heavy solid ones) due to soft γ rays are the same as in Fig. 3.

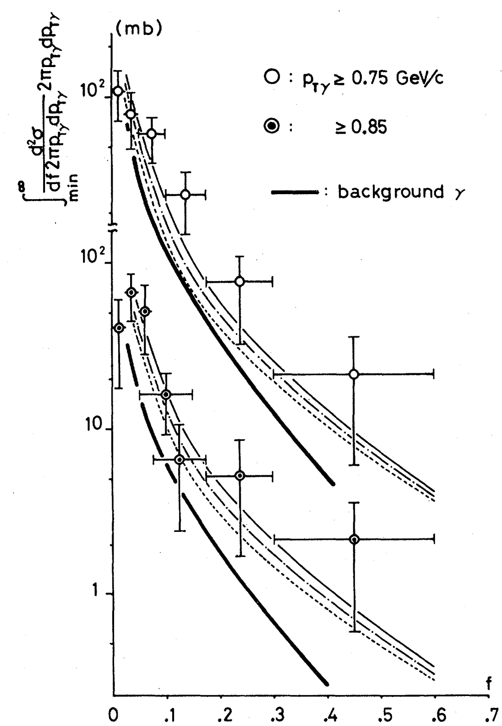

FIG. 22. Comparison of f distribution between the C-jet data and the theoretical calculations. Curves drawn there are the same as in Fig. 21.

with small $p_{T\gamma}$, our theoretical calculations based on QCD reproduce nicely the large-$p_{T\gamma}$ data in the region $p_{T\gamma} \gtrsim 0.75$ GeV/c obtained by two-story EC at the energy region $\sqrt{s} \sim 500$ GeV, if we choose appropriate sets for the parameters mentioned above.

One may worry about the experimental condition inherent in C-jet data, that is, the cms energy $\sqrt{s}$ is not constant, but variant around $400 \sim 960$ GeV with $\sqrt{s} = 523$ GeV, although our calculation is performed with the set $\sqrt{s} = 523$ GeV. It does not, however, yield serious trouble within such range of energy variation, because the effective number of partons (quark and gluon) in the target nucleon depends logarithmically on $\sqrt{s}$. For instance, let us show the dependence of the effective number of partons on $\sqrt{s}$ in Fig. 23, obtained with use of the present parametrization for $G_p(x, Q^2)$. As seen there, such variation of $\sqrt{s}$ does not bring us any significant effect for the present conclusion.

Another problem one may worry about is plural interaction in nucleus and in addition successive interaction in producer target with $\frac{1}{3}$ mean free path. The former contribution is, however, effective only in the backward cone, particularly at higher-energy region, as shown in recent accelerator experiments.[32] So we do not need to worry about this contamination, since the relevant range of emission angle is $\theta^* \lesssim 20°$ in forward cone.

The latter contribution also does not give serious effect against the present conclusion. One may think that as the thickness of the target layer used here is $\frac{1}{3}$ mean free path, the contamination of successive interactions is of the following magnitude:

$$\sum_{n=2}^{\infty} p_n(\tfrac{1}{3}) \Big/ \sum_{n=1}^{\infty} p_n(\tfrac{1}{3}) = 16\%, \tag{5.1}$$

where $p_n(x)$ denotes the Poisson function. This

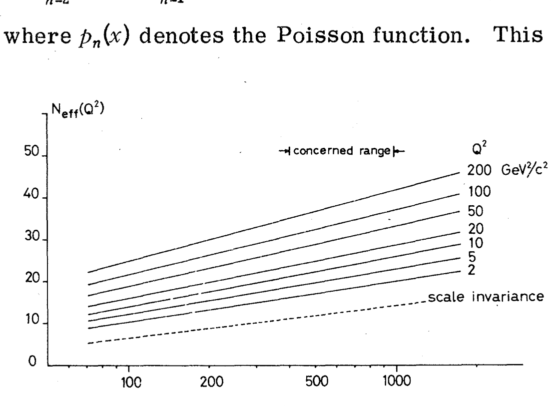

FIG. 23. Dependence of effective number of partons (quark+gluon) inside proton on $\sqrt{s}$ at various Q^2. Dashed straight line is the one expected from FF parametrization with $p^*_{\min} = 1$ GeV/c.

estimation is, however, not right, because we must take the fluctuations of k_γ into account, as well as the cutoff of the detection energy, both of which decrease the above estimate of contamination. That is, even if several interactions occurred in the target layer, the main interaction with the biggest energy flow $\sum E_\gamma$ is much more effective than the others, and in addition most γ rays coming from secondary interactions are cutoff by the minimum detection energy, say ~0.5 TeV.

On the basis of these considerations, we can say definitely that the choice of ${Q_0}^2 = 2$ GeV$^2/c^2$ and $p^*_{\min} = 1$ GeV, the essential parameters in the forward hard scattering of partons, gives reasonable agreement with the large-$p_{T\gamma}$ data in the cosmic-ray energy region $\sqrt{s} \sim 500$ GeV, assuming $B = 1.68$. Although we showed in the preliminary analysis[33] that the set of ${Q_0}^2 = 1$ GeV$^2/c^2$ with $B = 1$ also reproduce the C-jet data well, the values ${Q_0}^2$ and B chosen there seem unreliable from both viewpoints of theory and experiment, because $\alpha_s({Q_0}^2)$ is not small for ${Q_0}^2 = 1$ GeV$^2/c^2$, and one cannot neglect bias effects inherent in C-jet data.

If we assume $B = 2.0$ or 3.0, which correspond to the assumptions of $\langle k_\gamma \rangle_{\text{bias}} = \frac{1}{3}$ or $\frac{1}{2}$, respectively, the choice of ${Q_0}^2 = 3$ or 4 GeV$^2/c^2$ also gives agreement with C-jet data, as expected from Fig. 20. The choice for $p^*_{\min}$ is not serious here because of logarithmic dependence. So we can say in the present stage that the lower limit of Q^2, applicable for the quark-parton picture, lies around 2–4 GeV$^2/c^2$, where the running coupling constant $\alpha_s(Q^2)$ is small enough for the perturbation calculation in quark-gluon interactions.

Although the present paper is aimed to investigate "hard" γ rays with large $p_{T\gamma}$ from the viewpoint of quark-parton picture, one should also pay particular attention to the scale violation between ISR and C-jet data found in "soft" γ rays with small $p_{T\gamma}$, as shown in Fig. 7. One may think that it comes merely from the bias effect inherent in C-jet data, that is, the real value of bias factor B may be much larger than used here for $B = 1.66$ ($\langle k_\gamma \rangle_{\text{bias}} = 0.28$). The scale violation for soft γ rays is, however, inevitable between them even if we assume a higher value of B. For instance, the numerical constants presented in Eq. (2.18b) are

$$A = 4.01 \quad \text{with } z_{0\gamma} = 0.0583, \quad \text{for } B = 2 \quad (\langle k_\gamma \rangle_{\text{bias}} = \tfrac{1}{3}), \tag{5.2a}$$

$$A = 2.67 \quad \text{with } z_{0\gamma} = 0.0875, \quad \text{for } B = 3 \quad (\langle k_\gamma \rangle_{\text{bias}} = \tfrac{1}{2}), \tag{5.2b}$$

still giving a normalization twice that at $\sqrt{s} = 44.7$

GeV, even in the case of using extremely high values of B. According to Neuhofer *et al.*, the multiplicity of γ rays at ISR region is given, with use of Eq. (2.18a) by

$$\langle n_\gamma \rangle \simeq 4\pi A \langle p_{T\gamma} \rangle \ln(z_{0\gamma}\sqrt{s}/\langle p_{T\gamma}\rangle) = 9.4 \text{ at } \sqrt{s} = 44.7 \text{ GeV}, \quad (5.3a)$$

whereas in the C-jet region,

$$\langle n_\gamma \rangle = 43.8 - 55.2 \text{ at } \sqrt{s} = 523 \text{ GeV} \quad (5.3b)$$

for $\langle k_\gamma \rangle_{\text{bias}} = \frac{1}{4} \sim \frac{1}{3}$, much higher than the former. Of course, one must keep in mind that the above considerations are based on the assumption of Eq. (2.13), and a definite conclusion will be given by the forthcoming giant machines at Fermilab and CERN.

Phenomena of rapid increase of multiplicity, mostly coming from soft component, in the region $\gtrsim 10^{14}$ eV have already been pointed out by many physicists[34] on the basis of various cosmic-ray experiments. So, the results of Eqs. (5.3a) and (5.3b) are not surprising, but rather are matched with the prediction by cosmic-ray physicists.

The application of QCD for soft component is, of course, out of its range of validity, because of small Q^2, where interaction time ($\sim P/Q^2$) is much longer than the lifetime of virtual parton state inside proton ($\sim P/M_M{}^2$), so that the quark-parton picture is no more meaningful. So, we need a unified model, which may bring us deeper understanding for QCD, describing reasonable explanations for the relation between soft and hard components. In fact, EC data[11,19] indicate strong correlation between the above two, that is, C-jet events with large $p_{T\gamma}$ show high γ-ray multiplicity.

The investigation of the relation between soft and hard components, particularly on the jet structure found in target diagram, with use of the individual C-jet events, will be performed elsewhere.

ACKNOWLEDGMENTS

It is a pleasure to thank the members of Japan-Brazil emulsion-chamber collaboration for offering me numerous raw data on C jets. I would like to acknowledge useful discussions with Dr. N. Arata. In addition, thanks are also due to Professor Z. Arafune for useful comments to the present paper.

[1]M. Oda and Y. Tanaka, J. Phys. Soc. Jpn. 17, Suppl. A-III, 282 (1962); S. Miyake, K. Hinotani, and T. Kaneko, J. Phys. Soc. Jpn. 18, 592 (1963); T. Matano *et al.*, in *Proceedings of the 9th International Conference on Cosmic Rays, Calgary, 1967* [Can. J. Phys. 46, S56 (1968)]; Japan-Brazil Collaboration, Can. J. Phys. 46, 660 (1968).

[2]Japan-Brazil Collaboration, in *Proceedings of the Thirteenth International Conference on Cosmic Rays, Denver, 1973* (Colorado Associated University Press, Boulder, 1973), Vol. 3, p. 222.

[3]F. W. Busser *et al.*, Phys. Lett. 46B, 471 (1973).

[4]J. D. Bjorken and E. A. Paschos, Phys. Rev. 185, 1975 (1969); R. P. Feynman, in *High Energy Collisions*, edited by C. N. Yang *et al.* (Gordon and Breach, New York, 1969).

[5]R. D. Field and R. P. Feynman, Phys. Rev. D 15, 2590 (1977).

[6]S. J. Brodsky and G. Farrar, Phys. Rev. Lett. 31, 1153 (1973); R. Blankenbecler and S. J. Brodsky, Phys. Rev. D 10, 2973 (1974); J. Gunion, *ibid.* 10, 242 (1974).

[7]R. P. Feynman, R. D. Field, and G. C. Fox, Phys. Rev. D 18, 3320 (1978).

[8]R. E. Taylor, in *Proceedings of the International Conference on High Energy Physics, Tokyo, 1978*, edited by S. Homma, M. Kawaguchi, and H. Miyazawa (Phys. Soc. of Japan, Tokyo, 1979), p. 285; R. Wilson, *ibid.*, p. 306.

[9]E. M. Riordan *et al.*, Report No. SLAC-Pub-1634, 1975 (unpublished).

[10]D. P. Barber *et al.*, Phys. Rev. Lett. 43, 830 (1979); TASSO Collaboration, Report No. DESY 79/61, 1979 (unpublished).

[11]Japan-Brazil Collaboration, in *Sixteenth International Cosmic Ray Conference, Kyoto, 1979, Conference Papers* (Institute of Cosmic Ray Research, Univ. of Tokyo, Tokyo, 1979), Vol. 3, p. 362. After the conference, 14 more events of C-jet with $\sum E_\gamma \geq 20$ TeV were accumulated.

[12]For example, Brazil-Japan Collaboration, Prog. Theor. Phys. Suppl. 47, 1 (1971).

[13]Japan-Brazil Collaboration, Can. J. Phys. 46, S660 (1968).

[14]Brazil-Japan Collaboration, CKJ Report No. 13, 1975 from Cosmic Ray Laboratory, Univ. of Tokyo (unpublished). See also Ref. 2.

[15]For example, D. R. O. Morrison, Report No. CERN/D.Ph. II/Phys 73-11, 1973 (unpublished).

[16]V. V. Guseva *et al.*, J. Phys. Soc. Jpn. 17, Suppl. A-111 (1959) 375.

[17]For example, Japan-Brazil Collaboration, in *Proceedings of the Thirteenth International Conference on Cosmic Rays, Denver, 1973* (Colorado Associated University Press, Boulder, 1973), Vol. 3, p. 2219.

[18]R. W. Ellsworth, G. B. Yodh, and T. K. Gaisser, in *Cosmic Rays and Particle Physics—1978*, proceedings of the Bartol Conference, edited by T. K. Gaisser (AIP, New York, 1979); N. Arata, in *Sixteenth International Cosmic Ray Conference, Kyoto, 1979, Conference Papers* (Ref. 11), Vol. 6, p. 283.

[19]N. Arata, Nuovo Cimento 43A, 455 (1978).

[20]T. Shibata, CRL Report No. 53, 1977 (unpublished).

[21]D. H. Perkins and P. H. Fowler, Proc. R. Soc. London A218, 401 (1964).

[22]G. Neuhofer *et al.*, Phys. Lett. 38B, 51 (1972).

[23]E. Konishi, E. H. Shibuya, T. Shibata, and N. Tateyama, Prog. Theor. Phys. **56**,(No. 6) (1976).

[24]B. L. Combridge, J. Kripfganz, and J. Ranft, Phys. Lett. 70B, 234 (1977).

[25]R. Cutler and D. Sivers, Phys. Rev. D 16, 679 (1977).

[26]H. Georgi and H. D. Politzer, Phys. Rev. D 14, 1829 (1976); G. C. Fox, Nucl. Phys. B131, 107 (1977).

[27]V. Barger and R. J. N. Phillips, Nucl. Phys. B73, 269 (1974).

[28]See Fig. 4 of Ref. 7.

[29]Proposal by C. Rubbia *et al.*, Reports Nos. CERN/SPSC/78-06, 1978 and SPSC/P92, 1978 (unpublished).

[30]J. Kempa, J. Wdowczyk, and E. Zujewska, in *Proceedings of the Thirteenth International Conference on Cosmic Rays, Denver, 1973* (Colorado Associated University Press, Boulder, 1973), Vol. 3, p. 2145; R. A. Nam *et al.*, in *Proceedings of the Fifteenth International Conference on Cosmic Rays, Plovdiv, 1977*, edited by B. Betev (Bulgarian Academy of Sciences, Sofia, 1977), Vol. 8, p. 104. G. B. Yodh, Y. Pal and J. S. Trefil, Phys. Rev. Lett. 28, 1005 (1972).

[31]U. Amaldi *et al.*, Phys. Lett. 66B, 390 (1977); T. Yoshida, in *Sixteenth International Cosmic Ray Conference, Kyoto, 1979, Conference Papers* (Ref. 11), Vol. 7, p. 311.

[32]For example, W. Busza, in *Proceedings of the Seventh International Colloquium on Multiparticle Production, Tutzing, Germany, 1976*, edited by J. Benecke *et al.* (Max-Planck-Institute, Munich, Germany, 1976).

[33]T. Shibata, in *Sixteenth International Cosmic Ray Conference, Kyoto, 1979, Conference Papers* (Ref. 11), Vol. 7, p. 346.

[34]For example, G. B. Khristiansen, Rapporteur Talk at 14th International Cosmic Ray Conference, Munchen (1975). J. Wdowczyk, *ibid.* p. 4012.

[35]M. Dardo, S. Alessio, and K. Sitte, in *Sixteenth International Cosmic Ray Conference, Kyoto, 1979, Conference Papers* (Ref. 11), Vol. 7, p. 81.